Cell-line-specific network models of ER+ breast cancer identify PI3Kα inhibitor sensitivity factors and drug combinations

Jorge Gómez Tejeda Zañudo[1,2,*,#], Pingping Mao[2,3,*], Clara Alcon[4], Kailey J. Kowalski[2], Gabriela N. Johnson[2], Guotai Xu[5,6], José Baselga[5,6,%], Maurizio Scaltriti[5,6], Anthony Letai[2], Joan Montero[4,&,#], Reka Albert[7,8,&,#], and Nikhil Wagle[1,2,&,#].

1.- Eli and Edythe L. Broad Institute of MIT and Harvard, Cambridge, MA, 02142, USA
2.- Department of Medical Oncology, Dana-Farber Cancer Institute, Harvard Medical School, Boston, MA, 02115, USA
3.- Bluebird bio, Cambridge, MA, 02142, USA
4.- Institute for Bioengineering of Catalonia (IBEC), The Barcelona Institute of Science and Technology (BIST), Barcelona, Spain.
5.- Human Oncology & Pathogenesis Program, Memorial Sloan Kettering Cancer Center, New York, NY, 10065, USA
6.- Department of Pathology, Memorial Sloan Kettering Cancer Center, New York, NY, 10065, USA
7.- Department of Physics, The Pennsylvania State University, University Park, PA, 16802-6300, USA
8.- Department of Biology, The Pennsylvania State University, University Park, PA, 16802-6300, USA
%.- Present address: AstraZeneca, Gaithersburg, MD, USA.
*.- These authors are co-first authors
&.- These authors are co-senior authors
#.- To whom correspondence should be addressed: jgtz@broadinsitute.org (J.G.T.Z.), jmontero@ibecbarcelona.eu (J.M.), rza1@psu.edu (R.A.), nikhil_wagle@dfci.harvard.edu (N.W.).

Abstract

Durable control of invasive solid tumors necessitates identifying therapeutic resistance mechanisms and effective drug combinations. A promising approach to tackle the cancer drug resistance problem is to build mechanistic mathematical models of the signaling network of cancer cells, and explicitly model the dynamics of information flow through this network under distinct genetic conditions and in response to perturbations.

In this work, we use a network-based mathematical model to identify sensitivity factors and drug combinations for the PI3Kα inhibitor Alpelisib, which was recently approved for ER+ *PIK3CA* mutant breast cancer. We experimentally validate the model-predicted efficacious combination of Alpelisib and BH3 mimetics (e.g. MCL1 inhibitors), and the reduced sensitivity to Alpelisib caused by FOXO3 knockdown, which is a novel potential resistance mechanism. Our experimental results showed cell-line-specific sensitivity to the combination of Alpelisib and BH3 mimetics, which was driven by the choice of BH3 mimetics. We find that cell lines were sensitive to the addition of either MCL1 inhibitor S63845 alone or in combination with BCL-XL/BCL-2 inhibitor Navitoclax, and that the need for the combination of both BH3 mimetics was predicted by the expression of BCL-XL. Based on these results, we developed cell-line specific network models that are able to recapitulate the observed differential response to Alpelisib and BH3 mimetics, and also incorporate the most recent knowledge on resistance and response to PI3Kα inhibitors.

In conclusion, we present an approach based on the development, experimental testing, and refining of mathematical models, which we apply to the context of PI3Kα inhibitor drug resistance in breast cancer. Our approach predicted and validated PI3Kα inhibitor sensitivity factors (FOXO3 knockdown) and drug combinations (BH3 mimetics), and illustrates that network-based mathematical models can contribute to overcoming the challenge of cancer drug resistance.

Introduction

Overcoming intrinsic or acquired resistance to cancer drug therapies is one the biggest challenges faced today by patients, oncologists, and cancer researchers (Vasan, Baselga, and Hyman 2019; Konieczkowski, Johannessen, and Garraway 2018). This is particularly the case in the setting of metastatic disease, which accounts for the majority of cancer deaths (Steeg 2016; Weigelt, Peterse, and van ’t Veer 2005). The challenge underlying cancer drug resistance is exemplified by metastatic estrogen receptor positive (ER+) breast cancer, the most common type of metastatic breast cancer. Despite the availability of multiple lines of effective drug therapies (Waks and Winer 2019) (endocrine and targeted therapies, CDK4/6 inhibitors, among others), the tumor will eventually become resistant to all available treatments. As a result, long-term patient survival has not greatly improved, with a median prognosis of around 3-4 years (Caswell-Jin et al. 2018; Waks and Winer 2019).

One of the most recently approved drugs to treat ER+ breast cancer is Alpelisib (previously known as BYL719), which is a PI3Kα-specific inhibitor approved for the use in this type of cancer when it has activating *PIK3CA* mutations; Alpelisib is used in combination with Fulvestrant (a selective estrogen receptor degrader, a type of ER inhibitor) (André et al. 2019). Multiple lines of clinical evidence support PTEN loss-of-function as a clinically relevant resistance mechanism to Alpelisib and other PI3Kα inhibitors (Juric et al. 2015; Costa et al. 2020; Razavi et al. 2020). There are several other potential PI3Kα inhibitor resistance mechanisms that have been identified through *in vitro* or *in vivo* studies (Elkabets et al. 2013; Le et al. 2016; Castel et al. 2016; Costa et al. 2015; Schwartz et al. 2015; Bosch et al. 2015; Kodack et al. 2017; Donnella et al. 2018; Hopkins et al. 2018), but it is still an open question if these will drive resistance in patients and if they will be common enough to be clinically relevant. It is also likely that there are currently unidentified PI3Kα resistance mechanisms that will be found as the landscape of intrinsic and acquired resistance mechanisms is revealed, as has happened in the case of endocrine therapies (Razavi et al. 2018; Bertucci et al. 2019) and CDK4/6 inhibitors (Wander et al. 2020).

How can we identify these currently unknown PI3Kα resistance mechanisms? Based on what we have learned from other targeted drugs (e.g. BRAF(Lito, Rosen, and Solit 2013) or EGFR inhibitors(Sun and Bernards 2014)), resistance mechanisms act by reactivating the targeted pathway or by activating alternative oncogenic pathways that bypass it (Vasan, Baselga, and Hyman 2019; Konieczkowski, Johannessen, and Garraway 2018). Therefore, a promising avenue to identify such resistance mechanisms is to use approaches that combine a deep understanding of the oncogenic pathways driving ER+ *PIK3CA* mutant breast cancer, their cross-talk, and their integration by cancer cells to make the cellular decisions that result in tumor growth. One such approach is provided by mathematical models of cancer (Clarke and Fisher 2020; Rockne et al. 2019), particularly dynamic network models, which mechanistically model the dynamics of the molecular network underlying cancer cells (G. T. Zañudo, Steinway, and Albert 2018; Saez-Rodriguez and Blüthgen 2020).

Dynamic network models are based on mechanistic knowledge and explicitly model how information flows through signaling networks under distinct genetic conditions (e.g. in a context where known or potential

resistance mechanisms are active) and in response to perturbations (e.g. drugs or environmental signals). A particularly attractive property of dynamic network models in the context of cancer is that these models can be personalized to become cancer-cell-specific or tumor-specific by introducing known genetic alterations and/or by mimicking the known response (or lack thereof) to a perturbation (Saez-Rodriguez and Blüthgen 2020). Tested and validated network models can predict the degree of effectiveness of single-agent and combinatorial drug interventions, and predict potential mechanisms of drug resistance, which can then be used to prioritize drug combinations for *in vitro* and *in vivo* testing in relevant cancer model systems (G. T. Zañudo, Steinway, and Albert 2018; Saez-Rodriguez and Blüthgen 2020; Gómez Tejeda Zañudo, Scaltriti, and Albert 2017; Steinway et al. 2015; Béal et al. 2018; Fröhlich et al. 2018; Barrette, Bouhaddou, and Birtwistle 2018; Fey et al. 2015).

We previously built a network-based mathematical model of oncogenic signal transduction in ER+ *PIK3CA* mutant breast cancer. The model integrated the mechanistic knowledge of the response/resistance to PI3Kα inhibitors and other drugs relevant in the context of ER+ breast cancer (e.g. CDK4/6 inhibitors, ER inhibitors, or mTORC1 inhibitors). The model was based on the combined knowledge of *in vitro*, *in vivo*, and clinical literature; it recapitulated the drug resistance phenotype of a variety of resistance mechanisms to PI3Kα inhibitors (e.g. PTEN loss-of-function, mTORC1 activity, and PIM overexpression) and other drugs (e.g. RB1 loss in response to CDK4/6 inhibitors, and ER transcriptional reactivation in response to ER inhibitors). By exhaustively testing the effect of all single- and double-element perturbations, the model predicted potential resistance mechanisms and efficacious drug combinations for PI3Kα inhibitors. In particular, it predicted the knockdown of tumor suppressors FOXO3, RB1, or p21 and p27 as potential PI3Kα inhibitor resistance mechanisms, and identified BH3 mimetics targeting anti-apoptotic proteins MCL1, BCL-XL, and BCL2 as efficacious drug combinations.

In this work we experimentally test the above predictions of our mathematical model. We find that some of the model's predictions are verified experimentally, in particular, the efficacy of the drug combination of Alpelisib and BH3 mimetics, and the reduced sensitivity to PI3Kα inhibitors caused by FOXO3 knockdown. We also find some discrepancies between our experimental findings and the model, some of which are cell-line specific. In particular we find a cell-line specific response to BH3 mimetics in the most commonly used cell line models for ER+ *PIK3CA* mutant breast cancer, namely, MCF7 and T47D. Finally, we construct cell-line specific models that incorporate and recapitulate the most recent work on PI3Kα inhibitors (Hopkins et al. 2018; Donnella et al. 2018), including our experimental results.

Results

PI3Kα inhibitors and BH3 mimetics are a synergistically efficacious drug combination and induce apoptosis in ER+ *PIK3CA*-mutant breast cancer cell lines

In the network model, PI3Kα inhibition has a cytotoxic effect mediated by the increased activity of the pro-apoptotic BCL-2 family members BIM and BAD (respectively, through upregulation of FOXO3-mediated transcription and through a decrease of an inactivating AKT-mediated phosphorylation). The cytotoxic effect of PI3Kα inhibition is countered by the presence of anti-apoptotic BCL-2 family members MCL1 and BCL2 (which in the model represents BCL-2 and other anti-apoptotic family members such as BCL-XL). As a result, the combined inhibition of PI3Kα and anti-apoptotic family members (MCL1, BCL-2, or BCL-XL, each of which can be targeted using BH3 mimetics) is predicted to be an effective and synergistic drug combination. Specifically, the model predicts that inhibition of the anti-apoptotic family members would be more effective to induce

apoptosis than currently used (Fulvestrant) and proposed (Palbociclib, Everolimus) drug combinations, which predominantly inhibit cell proliferation.

To test the effect of PI3Kα inhibitors and BH3 mimetics of anti-apoptotic proteins, we first treated MCF7 cells (ER+, *PIK3CA*-mutant) with PI3Kα inhibitor Alpelisib and MCL1 inhibitor S63845 (a BH3 mimetic (Kotschy et al. 2016)) separately and in combination using both a long-term colony formation assay (2 weeks, Fig. 1A) and a short-term cell viability assay (6 days, Fig. 1B). In both cases the combination of Alpelisib and S63485 is more efficacious than each drug on its own. In particular, we calculate the synergy score of the combination using MuSyC (Wooten et al. 2019; Meyer et al. 2019) and find that it is synergistically efficacious ($\beta_{obs} = 0.45$, where $\beta_{obs} > 0$ means the combination is synergistically efficacious and $\beta_{obs,null} = 0.08$ is the null-hypothesis value expected from doubling the Alpelisib concentration). To compare the synergistic efficacy of the Alpelisib + S63845 combination with other proposed Alpelisib drug combinations (with Fulvestrant (André et al. 2019; Bosch et al. 2015), Palbociclib (Vora et al. 2014), Everolimus (Elkabets et al. 2013), among others), we performed drug response curves of the combination of Alpelisib with each of these other drugs and calculated their synergy score (Fig. 1C, Suppl. Fig. S1). We find that all the tested drug combinations were synergistically efficacious (i.e. $\beta_{obs} > 0$, with their range being 0.24 - 0.45; Fig. 1C), but the Alpelisib + S63845 combination had the highest synergy score among all the combinations ($\beta_{obs} = 0.45$).

To determine if the effect of the Alpelisib + S63845 combination is mediated by apoptosis or other mechanisms, we treated MCF7 with each drug separately and in combination, and measured the levels of cleaved PARP and total PARP (Fig. 1D). We find that Alpelisib + S63845 induces increased levels of cleaved PARP compared to each drug alone at both time points (8 and 24 h), with the effect being more evident at the early (8 h) time point (Fig. 1D). To contextualize the apoptotic effect of the Alpelisib + S63845 combination, we tested the effect of single agent and drug combinations and measured the resulting apoptotic priming using dynamic BH3 profiling (Montero et al. 2015) (Fig. 1E). We find that the Alpelisib + S63845 combination showed the highest percent increase in Δ% priming of all combinations, and that this effect was larger than each drug on its own. In particular, the Alpelisib + S63845 combination showed a higher Δ% priming than Alpelisib + Fulvestrant (recently approved for treatment for ER+ *PIK3CA*-mutant metastatic breast cancer (André et al. 2019; Bosch et al. 2015)) and Alpelisib + Everolimus (which had previously been found to increase Alpelisib-induced cell death (Elkabets et al. 2013)).

We also performed similar experiments in T47D cells, another ER+ breast cancer cell line. In contrast to MCF7, T47D cells did not show a strong synergistic effect under the combination of Alpelisib + S63845 (Fig. 2B, Suppl. Fig S2A). However, the addition of Navitoclax (a BH3 mimetic targeting BCL-XL and BCL-2) to the combination of Alpelisib and S63845 recapitulated the effects seen in the MCF7 cells (Fig. 2A-B). The Alpelisib + S63845 + Navitoclax combination had a strong synergistically efficacious effect ($\beta_{obs} = 1.10$; Fig. 2A) and had a significantly higher synergy score than other combinations tested (Fig. 2B). The combination of Alpelisib + S63845 + Navitoclax in T47D also showed increased apoptosis, measured by cleaved PARP and PARP, which is consistent with the results in MCF7 cells (Fig. 2D). The increased apoptosis was further confirmed by measuring cell death through Annexin V staining (Fig. 2C).

Given that the addition of BCL-XL/BCL-2 inhibitor Navitoclax sensitized T47D cells to the combination of Alpelisib + S63845, we reasoned that this was because T47D cells had a higher expression of BCL-XL and/or BCL-2 compared to MCF7 cells. To test this hypothesis, we looked at the gene and protein expression of MCF7 and T47D cells in the Cancer Cell Line Encyclopedia (CCLE) (Nusinow et al. 2020; Ghandi et al. 2019). Gene and protein expression of BCL-XL was higher in T47D compared to MCF7, consistent with our hypothesis (Supp. Fig S2B;$|\Delta\, log_2\,(TPM + 1)| = 1.68$, difference robust z-score $|z| = 1.08$; $|\Delta\, Relative\ protein\ expression| = 0.64$, difference robust z-score $|z| = 0.59$). For the case of BCL-2, there was

little difference in protein expression and the difference in gene expression was in the opposite direction of the effect we are trying to explain (higher gene expression in MCF7 compared to T47D vs increased sensitivity in T47D when adding Navitoclax) (Supp. Fig S5B;$|\Delta\ log_2\ (TPM+1)| = 4.14$, difference robust z-score $|z| = 2.19$;$|\Delta\ Relative\ protein\ expression| = 0.13$, difference robust z-score $|z| = 0.09$).

To further test whether BCL-XL expression can serve as a biomarker for cells that require inhibition of BCL-XL to become sensitive to MCL1 inhibitors, we looked at how the effect of MCL1 gene knockout correlated with gene expression using the CRISPR/Cas9 loss-of-function genetic screens of the Cancer Dependency Map (DepMap) (Meyers et al. 2017; Dempster et al. 2019). Consistent with the biomarker role of BCL-XL, sensitivity to MCL1 gene knockout was strongly correlated with BCL-XL expression (Fig. 2E; $Pearson\ correlation = 0.45$, $p = 1.9\ \times 10^{-37}$;$Spearman\ correlation = 0.47$, $p = 7.2\ \times 10^{-41}$) and this was the strongest gene expression correlate (Pearson) among all genes. There was no strong correlation between sensitivity to MCL1 gene knockout and MCL1 ($Pearson\ correlation = -0.03$, $p = 4.3\ \times 10^{-1}$;$Spearman\ correlation = -0.03$, $p = 3.6\ \times 10^{-1}$) or BCL-2 expression ($Pearson\ correlation = -0.15$, $p = 4.3\ \times 10^{-5}$;$Spearman\ correlation = -0.10$, $p = 8.4\ \times 10^{-3}$). Consistent with our experimental findings, MCF7 is in the low end of BCL-XL expression (Fig. 2E;$log_2\ (TPM+1) = 5.50$, robust z-score $z = -0.62$) and is sensitive to MCL1 gene knockout (Fig. 2E; $gene\ effect\ = -1.06$, where a $gene\ effect$ of 0 means no effect, while a $gene\ effect$ of -1 means the same effect as an essential gene). T47D is in the high end of BCL-XL expression (Fig. 2E; $log_2\ (TPM+1) = 7.19$, robust z-score $z = 0.94$) and, although it is not in the DepMap database, the inferred sensitivity to MCL1 gene knockout is less than half of that for MCF7 (Fig. 2E; $median(gene\ effect) = -0.40$ for the 57 cell lines within $\pm 2.5\%$ of the $log_2\ (TPM+1)$ of T47D's MCL1 gene expression). We also find consistent results for the effect of MCL1 gene knockout and BCL-XL expression when looking at other loss-of-function (RNAi) screen datasets (Supp. Fig. S2C), although the dynamic range of gene effects for MCL1 is much smaller for the RNAi case.

In summary, these results support the predictions of the model, (1) the combined inhibition of PI3Kα and the relevant anti-apoptotic family members (MCL1 for MCF7; MCL1 and BCL-XL for T47D) is an effective and synergistic drug combination, and (2) combined Alpelisib and BH3 mimetics have a larger cell death effect than each drug alone and other effective drug combinations (Alpelisib + Everolimus, Alpelisib + Fulvestrant).

FOXO3 knockdown is a potential resistance mechanism to PI3Kα inhibitors

In the network model, PI3Kα inhibition increases FOXO3 nuclear localization and transcriptional activity through AKT-mediated dephosphorylation of FOXO3 [(Brunet et al. 1999; Castel et al. 2016; Muranen et al. 2012; Chandarlapaty et al. 2011)]. Increased FOXO3 nuclear activity upregulates the expression of downstream targets that result in the suppression of cell growth and induction of cell death (Hu et al. 2004; Brunet et al. 1999; Medema et al. 2000; Castel et al. 2016). As a result, the network model predicts that knockdown of FOXO3 is a potential resistance mechanism to PI3Kα inhibitors and that this reduced sensitivity is a result of blocking FOXO3 transcriptional activity.

To test this prediction, we generated MCF7 and T47D cell lines with FOXO3 knockdown using CRISPR-Cas9 technology and verified the knockdown of FOXO3 by western blot (Fig. 3A). We tested the response of FOXO3 KD MCF7 and T47D cells to two PI3Kα inhibitors (Alpelisib and Taselisib) and find that both cell lines show reduced sensitivity to both PI3Kα inhibitors when compared to control cells with NT sgRNA (Fig. 3B; two-sided t-test $p < 0.01$for each sgRNA vs NT control comparison, fold change 1.4 - 2.2 compared to NT control for MCF7, fold change 1.4 - 1.5 compared to NT control for T47D). To further test this reduced sensitivity to PI3Kα inhibitors, we performed drug response curves in response to Alpelisib and Taselisib (Fig. 3C-D). We find that

the drug response curves of FOXO3 KD MCF7 show a clear separation from the control curves (Fig. 3C), consistent with the resistant phenotype in Fig. 3B. For FOXO3 KD T47D cells we do not see significant effect on PI3Kα inhibitor sensitivity from FOXO3 knockdown (Fig. 3D), a result that may be attributed to the methodology being insufficiently sensitive to measure moderate effects. (Supp. Fig. S3).

Many drug resistance mechanisms for targeted therapies involve reactivation of the signaling pathway inhibited by targeted therapy. According to the model, FOXO3 KD does not reactivate the PI3K pathway, and we decided to test this experimentally by measuring AKT phosphorylation. We find that that AKT(S473) phosphorylation was similar when comparing FOXO3 KD and control cells at baseline or in response to Alpelisib, and that similar results were observed in both MCF7 and T47D (Fig. 3E). We conclude that FOXO3 KD does not reactivate PI3K pathway activity. This is consistent with the current knowledge on FOXO3, (which indicates that it mainly acts downstream of the PI3K pathway but might also act upstream of the PI3K pathway due to feedback activation) and suggests that the effect of feedback activation by FOXO3 is weak in this context.

One important prediction of the model is that FOXO3 KD reduces PI3Kα inhibitor sensitivity by decreasing drug-induced apoptosis. To test this, we determined the effect of Alpelisib on cell death by measuring the levels of cleaved PARP and PARP in FOXO3 KD vs control cells (Fig. 3E). We find that the FOXO3 KD MCF7 cells have reduced levels of cleaved PARP compared to control (Fig. 3E, left). We do not see this difference in cleaved PARP for T47D (Fig. 3E, right). The reduced levels of cleaved PARP seen only in MCF7 FOXO3 KD cells is consistent with the reduced cytotoxic effect seen in the Alpelisib drug response curves of FOXO3 KD in MCF7 but not in T47D (Fig. 3C-D).

Overall, we find that FOXO3 KD reduces sensitivity to PI3Kα inhibitors in both cell lines, and that this effect is mediated by a reduction in drug-induced apoptosis in MCF7 cells. These results are consistent with the predictions of the model and suggest that downregulation of FOXO3 is a potential resistance mechanism for PI3Kα inhibitors.

CDKN1B (p27) knockdown does not have a strong effect on PI3Kα inhibitor sensitivity

The network model contains a node, $p21/p27$, that merges the tumor suppressor CDKN1B (p27) and its paralogue CDKN1A (p21). In the model, PI3Kα inhibition results in an increased activity of this node, mediated by the upregulation of FOXO3-mediated *CDKN1B* transcription (Medema et al. 2000) and a decrease in AKT-mediated p27 and p21 phosphorylation (Viglietto et al. 2002; Liang et al. 2002; Zhou et al. 2001). p27 and p21 exert their tumor suppressor function by binding and inactivating the cyclin E-CDK2 complex (Sherr and Roberts 1999; Polyak et al. 1994; Wander, Zhao, and Slingerland 2011; Planas-Silva and Weinberg 1997), which upon release from p27 or p21 promotes the G1-S transition and progression into the cell cycle. As a consequence, the model predicts that inactivation of the merged $p21/p27$ node will interfere with the cytostatic effect of PI3Kα inhibition, and result in a reduced sensitivity to PI3Kα inhibitors. As the model does not specify the contribution of p27 and p21 to this merged node, inactivation of this merged node could be reproduced by knockdown of CDKN1B (if the contribution of p21 is minor) or only by simultaneous knockdown of CDKN1B and CDKN1A. Given that p27 but not p21 has been shown to be transcriptionally upregulated by AKT-mediated FOXO3 activation (Medema et al. 2000; X. Zhang et al. 2011), we choose to test the effect of p27 knockdown.

We generated MCF7 and T47D cell lines with CDK1NB knockdown, which we verified through western blotting (Fig. 4A). We then tested the response of sgRNA CDKN1B cells to the PI3Kα inhibitors Alpelisib and Taselisib (Fig. 4B-C). We find that the CDKN1B KD cell lines did not show a consistent reduced sensitivity to PI3Kα

inhibition compared to control, neither in the drug response curves nor in the further optimized drug treatment experiment at selected doses. (Fig. 4C).

The lack of a strong effect of CDKN1B (p27) on PI3Kα inhibitor sensitivity can still be consistent with the model, if we hypothesize that only joint KD of p21 and p27 can accomplish what we observe in the model for the inactivation of the node $p21/p27$. To test the plausibility of this hypothesis, we looked at the gene expression and gene knockout effect of p21 and p27 using the Cancer Cell Line Encyclopedia (CCLE) and the CRISPR/Cas9 loss-of-function genetic screens of the Cancer Dependency Map (DepMap). Across all cell lines, p21 tends to show a tumor suppressor effect ($median(gene\ effect) = 0.20$ for all 739 cell lines) and this effect is correlated with the cell line's p21 (*CDKN1A*) gene expression ($Pearson\ correlation = 0.48$, $p = 1.5 \times 10^{-43}$;$Spearman\ correlation = 0.47$, $p = 2.4 \times 10^{-41}$). This is not case for p27, which does not show a consistent tumor suppressor effect ($median(gene\ effect) = -0.01$for the for all 739 cell lines) and its effect is not correlated with its gene expression ($Pearson\ correlation = 0.05$, $p = 1.9 \times 10^{-1}$;$Spearman\ correlation = 0.08$, $p = 2.7 \times 10^{-2}$).

We also used the DepMap and CCLE database to look at whether we expect p21 knockout to show a difference between the MCF7 and T47D cell lines. MCF7 is in the high end of p21 gene expression (Fig. 4E;$log_2\ (TPM + 1) = 7.21$, robust z-score $z = 0.86$) and grows faster in response to CDKN1A gene knockout (Fig. 4E; $gene\ effect = 0.50$). T47D is in the low end of p21 expression (Fig. 4E; $log_2\ (TPM + 1) = 4.33$, robust z-score $z = -0.54$) and, although it is not in the DepMap database, the inferred effect of p21 gene knockout on T47D is less than half of that for MCF7 (Fig. 4E; $median(gene\ effect) = 0.17$ for the 23 cell lines within $\pm 2.5\%$ of the $log_2\ (TPM + 1)$ of T47D's *CDKN1A* gene expression).

Overall, our experimental results suggest that CDK1NB (p27) knockdown does not have a strong effect on PI3Kα inhibitor sensitivity, in contrast with what the network model predicts. Based on computational analysis of gene expression and loss-of-function cell line databases, we find that the lack of a strong effect seen in p27 knockout could be explained by the activity of p21 (CDKN1A); we expect MCF7 to show a stronger tumor suppressor effect than T47D in response to p21 knockout.

RB1 knockdown reduces sensitivity to PI3Kα inhibitors in a cell-line-specific manner

In the network model, PI3Kα inhibitors result in reduced cell proliferation by two mechanisms: by a decrease in E2F1 activity mediated by Rb or by a decrease in translational machinery mediated by mTORC1. As a result, the model predicts that RB1 knockdown would increase E2F1 activity and reduce the sensitivity to PI3Kα inhibition. To test this, we use T47D and MCF7 cell lines with sgRNA CRISPR KD of RB1 we previously generated (Wander et al. 2020).

Fig. 5A-B shows the drug response curve of sgRNA RB1 T47D and MCF7 cell lines in response to PI3Kα inhibitor Alpelisib. T47D RB1 KO cells show a reduced sensitivity to Alpelisib compared to control cells (Fig. 5A) and this reduced sensitivity is not seen in MCF7 cells (Fig. 5B). To further verify the reduced sensitivity to PI3Kα inhibitors in T47D RB1 KD cells, we used a long-term colony formation assay (Fig. 5C-D). This assay also indicates that T47D RB1 KD but not MCF7 RB1 KD cells (Fig. 5C) show reduced sensitivity to Alpelisib (Fig. 5D). In summary, we find that RB1 KD can reduce the sensitivity to PI3Kα inhibitor Alpelisib, as predicted by the model, and that this effect is cell-line-specific (T47D but not MCF7).

Cell-line-specific network models reproduce the efficacy of PI3Kα inhibitor drug combinations and resistance mechanisms

Our experimental results are in agreement with the model-predicted efficacy of combining PI3Kα inhibitors with BH3 mimetics and the reduced PI3Kα inhibitor sensitivity that results from FOXO3 knockdown or RB1 knockdown. However, our experimental results also exhibit cell-line-specific aspects, which the model does not fully recapitulate. For example, MCF7 cells were sensitive to combined Alpelisib and S63845 (Fig. 1) while T47D cells were only sensitive to combined Alpelisib, S63845, and Navitoclax (Fig. 2). To address this, we generated cell-line-specific network models for MCF7 and T47D.

The cell-line-specific models are based on an updated version of the network model that incorporates new knowledge generated on ER+ breast cancer drug resistance since the previous model was published (e.g. (Hopkins et al. 2018; Donnella et al. 2018; Wander et al. 2020)) and the discrepancies from the model found by our experimental results (see Supplemental Text). The updated network model separates protein pairs (p21 and p27, BCL-2 and BCL-XL) that were previously denoted by a single combined node (p21/p27 and BCL2). The updated model includes a new node that denotes the transcriptional status of MYC targets (following the results from (Ilic et al. 2011; Donnella et al. 2018)) and assumes that the mTORC1 and Rb-E2F pathways do not contribute equally to the response to Alpelisib (following our findings on RB1 and p27 knockdown). A condensed representation of the updated model is shown in Fig. 6A while a more complete representation of the model and the changes introduced is shown in Supp. Fig. 4A. This model describes the biological outcomes of proliferation and apoptosis using the multi-state nodes $Proliferation$ and $Apoptosis$ (each of which has 3 states) and their normalized propensities denoted by $Proliferation_{norm}$ and $Apoptosis_{norm}$(which take values between 0 and 1).

The MCF7-specific and T47D-specific network models differ only in three aspects: (1) the node denoting basal expression of BCL-XL is active in T47D but not MCF7 (in agreement with Fig. 2E), (2) the node denoting basal expression of p21 is more active in MCF7 than in T47D (in agreement with Fig. 4E), and (3) the contribution of the lowest active $Apoptosis$ state to $Apoptosis_{norm}$ is larger in MCF7 than T47D (i.e., $Apoptosis = 1$results in $Apoptosis_{norm} = 0.25$ in MCF7 and $Apoptosis_{norm} = 0.125$ in T47D) (in agreement with Figs. 1D and 2E).

The cell-line-specific models' cancerous states (which are steady states) and the timecourse of their response to Alpelisib share many similarities with that of the previous model. The cancerous states have active RTK, PI3K, MAPK, AKT, mTORC1, and ER signaling, which result in high survivability ($Proliferation_{norm} = 1$ and $Apoptosis_{norm} = 0$). These states can be primed for cell death, a common feature of cancer cells (Ni Chonghaile et al. 2011; Montero et al. 2015), by having pro-apoptotic protein BIM active but an anti-apoptotic protein counteracting its effect (BCL-2, BCL-XL, or MCL1 in the updated model). The time course of the MCF7-specific model in response to Alpelisib starting from a cancerous state is shown in Supp. Fig S4B. In response to Alpelisib, there is a quick inactivation of the MAPK, AKT, and mTORC1 pathways in both cell line-specific models, followed by the activation of FOXO3, which transcriptionally upregulates HER3 and ESR1. The inhibition of the mTORC1 pathway downregulates the node $MYC\ targets$, which results in reduced proliferation ($Proliferation_{norm} = 0.25$) in both models. The activation FOXO3 and inactivation of AKT results in the activation of pro-apoptotic proteins BIM and BAD, which result in a small increase in cell death ($Apoptosis_{norm} = 0.25\ in\ MCF7\ and\ Apoptosis_{norm} = 0.125\ in\ T47D$).

These cell-line-specific network models reproduce the observed difference in cell death response to BH3 mimetics and their combination with Alpelisib in each cell (see Fig. 6B and Supp. Fig S6, where $\Delta Apoptosis_{norm}$ is the difference with respect to the case of no perturbation). In the MCF7 model, Alpelisib

alone has a small effect on apoptosis ($\Delta Apoptosis_{norm} = 0.25$), S63845 alone has larger effect on apoptosis ($\Delta Apoptosis_{norm} = 0.68$), and combined Alpelisib and S63845 have the largest effect ($\Delta Apoptosis_{norm} = 1$) (Fig. 6B-C). In the T47D model, Alpelisib alone has a small effect on apoptosis ($\Delta Apoptosis_{norm} = 0.125$), S63845 or Navitoclax alone have no effect ($\Delta Apoptosis_{norm} = 0$), their combination has a larger effect ($\Delta Apoptosis_{norm} = 0.68$), and their combination with Alpelisib has the largest effect ($\Delta Apoptosis_{norm} = 1$) (Fig. 6B and Supp. Fig S5B).

The cell-line-specific models recapitulate how FOXO3 knockdown reduces sensitivity to Alpelisib in both MCF7 (Fig. 6D-E) and T47D (Fig. 6D and Supp. Fig S5D), and the stronger reduction in apoptosis seen in MCF7 (Fig. 6D). For the case of Rb knockdown and p21/p27 knockdown, the models reproduce the observations that their effect on sensitivity to Alpelisib is small ($Proliferation_{norm} = 0.25$ to $Proliferation_{norm} = 0.5$) and that p27 knockdown alone does not have a strong effect (no change in $Proliferation_{norm}$), and also incorporate the hypothesis that the effect of p21 and p27 requires knockdown of both p21 and p27 (Fig. 6D).

The MCF7-specific and T47D-specific network models recapitulate the PI3K inhibitor resistance mechanisms and drug combinations that the previous model did. For example, knockdown of PTEN, knockdown of TSC, or high expression of PIM make the cell insensitive to Alpelisib ($Proliferation_{norm} = 0.25$ with Alpelisib changes to $Proliferation_{norm} = 1$ with the addition of any of these resistance mechanisms), and the addition of Fulvestrant to Alpelisib results in a larger effect than any of them alone ($Proliferation_{norm} = 0.25$ with Alpelisib or Fulvestrant alone changes to $Proliferation_{norm} = 0$ with both) (Fig. 6D and Supp. Fig S5A and C) . Additional resistance mechanisms to Alpelisib or PI3K inhibitors that both models reproduce include high expression of SGK1/PDK1 (Castel et al. 2016), the HER3 microenvironment (Kodack et al. 2017), high activity of IGF1R and insulin (Hopkins et al. 2018), upregulation of ESR1 expression (Bosch et al. 2015), and high MYC activity (Ilic et al. 2011) (Supp. Fig S5C). The models also recapitulate the resistance mechanisms of other drugs. For example, Rb knockdown is a resistance mechanism to Palbociclib (Herrera-Abreu et al. 2016) ($Proliferation_{norm} = 0.25$ with Palbociclib changes to $Proliferation_{norm} = 1$ with added Rb knockdown) but has little effect in the presence of Fulvestrant (Wander et al. 2020) ($Proliferation_{norm} = 0.25$ with Fulvestrant to $Proliferation_{norm} = 0.5$ with the addition of Rb knockdown) (Supp. Fig S5C).

Overall, the cell-line specific network models we developed are able to reproduce the current knowledge of PI3Kα inhibitor resistance mechanisms and drug combinations, including the new results from this work on the efficacy of the combination of Alpelisib with BH3 mimetics and the reduced sensitivity to PI3Kα inhibitors as a result of FOXO3 knockdown.

Discussion

In this work, we experimentally validated several PI3Kα inhibitor drug resistance and sensitivity factors predicted by a network-based mathematical model of oncogenic signaling in ER+ *PIK3CA* mutant breast cancer. We experimentally verified (i) the efficacy of combining PI3Kα inhibitor Alpelisib with BH3 mimetics (MCL1 inhibitor S63845 alone or in combination with BCL-XL/BCL-2 inhibitor Navitoclax, in a cell-line specific manner), a promising PI3Kα inhibitor drug combination (Figs. 1 and 2) and (ii) the reduced sensitivity to PI3Kα inhibitors (Alpelisib and Taselisib) caused by FOXO3 knockdown, a novel candidate resistance mechanism for PI3Kα inhibitors (Fig. 3). We additionally found discrepancies with the model, in particular, our experiments found that the effect of p27 knockdown and RB1 knockdown did not result in the expected reduced sensitivity or had only a small cell-line specific effect (Figs. 4 and 5). Based on these experiments, we developed cell-line specific network models that can recapitulate our new results and other recent work on PI3Kα inhibitor drug resistance.

Our combined mathematical modeling and experimental approach follows the model/experiment refinement cycle that is a cornerstone of systems biology research (Coutant et al. 2019; Alberghina and Westerhoff 2007), and successfully applies it to the field of cancer drug resistance. In this approach, the cancer biology and clinical knowledge is integrated to form a model, experiments are performed to test and refine the model, which leads to new knowledge being generated, and to the cycle being repeated again. This completion of a model/experiment cycle is a step that is necessary for the development of predictive and validated mathematical models in cancer and systems biology, yet it is rarely accomplished (Coutant et al. 2019; Brady and Enderling 2019; Alberghina and Westerhoff 2007).

An important result from this work is that the combination of PI3Kα inhibitor Alpelisib with BH3 mimetics is synergistically efficacious and that this combination leads to an increase in apoptosis compared to any of them alone (Figs. 1 and 2). We find that the ideal choice of BH3 mimetics depends on the anti-apoptotic BCL-2 family members that are highly expressed in cancer cells (e.g. MCL1, BCL-XL, and BCL-2). For the case of T47D cells, which have high BCL-XL expression, Alpelisib was synergistically efficacious only when combined with MCL1 inhibitor S63845 and BCL-XL/BCL-2 inhibitor Navitoclax. Meanwhile, for MCF7 cells, which have low BCL-XL expression, Alpelisib was synergistically efficacious when combined with S63845 alone.

These cell-line specific results highlight an important lesson for the use of Alpelisib and BH3 mimetics in the clinical setting of breast cancer: fully taking advantage of this drug combination will require determining the relevant anti-apoptotic BCL-2 family dependence in the tumor. This could be accomplished by directly quantifying these BCL-2 family members in the tumor and/or by using functional genomic approaches such as dynamic BH3 profiling (Montero et al. 2015; Montero et al. 2019; Bhola et al. 2020). In line with this view, recent clinical trials on breast cancer tumors with high BCL-2 expression have focused on the combination of approved breast cancer therapies with BCL-2 inhibitor Venetoclax and have shown promising results (Whittle et al. 2020; Lok et al. 2019). Our results suggest an approach similar to the one used in these trials but using the combination of Alpelisib and tumor-specific BH3 mimetics determined through dynamic BH3 profiling.

Another key result from this work is that FOXO3 knockdown reduces the sensitivity to PI3Kα inhibitors, making it a novel candidate resistance mechanism (Fig. 3). FOXO3 exemplifies the unique insights that can be obtained from network models and their ability to integrate the context-dependent role of cancer-related genes. FOXO3 is known for its dual role as tumor suppressor and oncogene, acting as one or the other depending on the context. Previous work had highlighted FOXO3's role as an oncogene through its PI3K-inhibitor-induced feedback activation and the resulting upregulation of ESR1 and HER3. The upregulation of these receptors lead to increased survival in microenvironments that favor their signaling (Kodack et al. 2017; Bosch et al. 2015). Our network modeling and experimental findings show that the tumor suppressor effect of FOXO3 can dominate.

Overall, we successfully applied a systems biology approach combining a network-based mathematical model and its experimental validation to the problem of PI3Kα inhibitor drug resistance in ER+ *PIK3CA* mutant breast cancer. The result was the experimental validation of BH3 mimetics as an efficacious drug combination and of FOXO3 knockdown as a drug sensitivity factor and potential resistance mechanism. These results led to a refinement of the model and the development of cell-line specific network models that recapitulate the current knowledge on drug resistance to PI3Kα inhibitors. The validated drug combinations and sensitivity factors of our approach illustrate how the use of network modeling and systems biology approaches can contribute to overcoming the challenge of cancer drug resistance.

Acknowledgements

J.G.T.Z. would like to thank all members of the Wagle lab and all members of the Stand Up To Cancer – National Science Foundation Drug Combination Convergence Research Team for many useful discussions. J.G.T.Z. would also like to thank Stand Up To Cancer and V foundation staff, grant reviewers, and scientific leadership for organizing and making possible multiple meetings, which shaped and enriched this work. J.M. acknowledges support from the Ramon y Cajal Programme, Ministerio de Economia y Competitividad (RYC-2015-18357). J.M. and C.A. acknowledge the CELLEX foundation. This work was supported by the National Science Foundation grants PHY 1545832 (to R.A.), PHY 1545839 (to A.G.L. and N.W.) and 1545853 (to M.S. and G.X.), the Stand Up to Cancer Foundation, and Stand Up to Cancer Foundation/The V Foundation Convergence Scholar Awards to J.G.T.Z. (D2015-039), J.M. (D2015-037), and P.M..

Competing interests

P.M. is an employee of Bluebird bio. J.B. is an employee of AstraZeneca; is on the Board of Directors of Foghorn; and is a past board member of Varian Medical Systems, Bristol-Myers Squibb, Grail, Aura Biosciences, and Infinity Pharmaceuticals. He has performed consulting and/or advisory work for Grail, PMV Pharma, ApoGen, Juno, Eli Lilly, Seragon, Novartis, and Northern Biologics. He has stock or other ownership interests in PMV Pharma, Grail, Juno, Varian, Foghorn, Aura, Infinity Pharmaceuticals, and ApoGen, as well as Tango and Venthera, of which he is a cofounder. He has previously received honoraria or travel expenses from Roche, Novartis, and Eli Lilly. J.B. is an employee of AstraZeneca, which is currently developing capivasertib, an AKT inhibitor. J.B. is a past board member of Infinity Pharmaceuticals, which markets duvelisib and IPI-549. J.B. has been a paid consultant and/or advisor for Novartis, which markets alpelisib, buparlisib, and everolimus. J.B. has stock or other ownership interests in Venthera (of which he is a cofounder), which is developing topical PI3K inhibitors for dermatological conditions. Companies that have developed or are developing PI3K inhibitors, for which coauthors on this study have a disclosure, include Novartis, AstraZeneca, Eli Lilly, Roche, Infinity Pharmaceuticals, and Venthera. J.B. is an inventor on a patent application (PCT/US2019/047879) submitted by MSKCC that is related to the use of multiple PIK3CA mutations as a biomarker for clinical response to PI3K inhibitors. M.S. is on the scientific advisory board of Menarini Ricerche and the Bioscience Institute; has received research funds from Puma Biotechnology, Daiichi-Sankio, Targimmune, Immunomedics, and Menarini Ricerche; and is a cofounder of Medendi.org. M.S. has received research funds from Menarini Ricerche, which markets MEN1611. A.G.L. reports consulting for AbbVie, sponsored research by Novartis, AbbVie, Astra-Zeneca, and being a co-founder of Flash Therapeutics and Vivid Bioscience. J.M. reports previous consulting for Vivid Biosciences and Oncoheroes Biosciences. N.W. reports the following prior relationships: Foundation Medicine (consultant, stockholder), Novartis (consultant, grant support, advisory board). N.W. reports the following current relationships: Puma Biotechnologies (grant support), Eli Lilly (consultant/advisory board), Section 32 (scientific advisory board), Relay Therapeutics (scientific advisory board, stockholder). No potential conflicts of interests were disclosed by the other authors.

Methods

Cell culture

293T, T47D and MCF7 cells were purchased from American Type Culture Collection (ATCC). 293T cells were cultured in DMEM (GIBCO #11995-065) with 10% fetal bovine serum (Gemini #100-119). T47D cells were

cultured in Phenol Red-free RPMI-1640 (GIBCO #11835-030) with 10% FBS. MCF7 cells were cultured in Phenol Red-free MEM-α (GIBCO #41061-029) with 10% FBS.

Drug treatment

Drugs that were used to treat cells include Taselisib (Selleck Chemicals # S7103), Alpelisib (Selleck Chemicals # S2814), S63845, Everolimus (Selleck Chemicals # S1120), Navitoclax (Selleck Chemicals # S1001), Fulvestrant (Sigma Aldrich # I4409), Ipatasertib (Thermo Fisher Scientific # NC0742252), Palbociclib (Selleck Chemicals #S1116).

Generation of plasmids and engineered cells

We cloned sgRNA into lentiCRISPRv2 vector (gift from Dr. Adam Bass's laboratory) and lentivirus was produced in 293T cells using psPAX2 and pCMV-VSV-G plasmids. T47D or MCF7 cells were infected with lentivirus to derive stable cell lines expressing sgRNA to target FOXO3 (FOXO3_1: CGCCGACTCCATGATCCCCG, FOXO3_2: GGAAGAGCGGAAAAGCCCCC) or CDKN1B (CDKN1B_1: GGAGAAGCACTGCAGAGACA, CDKN1B_2: GGACCACGAAGAGTTAACCC) or non-targeting sgRNA controls (NT_0: GTATTACTGATATTGGTGGG, NT: ACGGAGGCTAAGCGTCGCAA). The sequences for the guides for FOXO3 and CDKN1B were obtained from the DepMap 18Q3 release. Cells were selected by puromycin (Life Technologies #A1113803). RB1 and CRISPR non-targeting guide cells used as control for RB1-related experiments were obtained as a gift from Flora Luo and the Garraway laboratory, and have been previously characterized (Wander et al. 2020).

Kill curves and CellTiter-Glo viability assay

Cells were plated in 96-well tissue culture ViewPlate (Perkin Elmer # 6005181) on Day 1 and treated with drug on Day 2. Media with or without drugs was refreshed on Day 5. On Day 8, cells were equilibrated to room temperature, media was removed, and cells were lysed in a mixture of 50 µL media and 50 µL CellTiter-Glo 2.0 reagent (Promega # G9243) per well. Plates were then incubated on an orbital shaker for 2 mins. Following another 10 mins of incubation at room temperature to stabilize signal, luminescence was recorded to measure cell viability on Infinite M200 Pro microplate reader (Tecan).

Western blotting

Cell lysates were prepared in RIPA buffer (Sigma Aldrich # R0278) supplemented with dithiothreitol (Life Technologies # 15508013), phenylmethane sulfonyl fluoride (Sigma Aldrich # P7626), protease inhibitor cocktail (Sigma Aldrich # P8340) and phosphatase inhibitor tablets (Roche # 4906845001). NuPAGE 4-12% Bis-Tris Midi protein gels (Invitrogen # WG1402A) were used for western blot. After electrophoresis, gel was transferred using Trans-Blot Turbo PVDF or nitrocellulose transfer pack (Bio-Rad # 1704158 and # 1704156). Membranes were probed with specific primary antibodies at 4 °C overnight and then incubated with corresponding HRP-conjugated secondary antibodies. We use Pierce ECL Plus Western Blotting Substrate (Thermo Fisher Scientific # 32132X3) as developing reagent.

Primary antibodies used in this study are: FOXO3 (CST #2497S), CDKN1B (CST #3698S), p-AKT (CST #12694S), pS6 (CST #4857S), MCL (CST #5453S), PARP (CST #9532S), cleaved PARP (CST #5625S), Actin (C4) (SC-47778). Secondary antibodies are from Invitrogen (anti-mouse A16090, anti-rabbit 32260, anti-goat 81-1620).

Colony formation assay

1,000-10,000 cells were plated in 6-well plates on Day 1 and treated on Day 2. Media was refreshed every 3-4 days until crystal violet staining. On the day of staining, cells were fixed with ice-cold 100% methanol for 10 minutes and then incubated with 0.5% crystal violet solution (Sigma Aldrich #C6158) in 25% methanol at room temperature for 10 minutes.

Cell death assays

Cells were treated as indicated and stained with fluorescent conjugates of annexin-V and PI (1 µg/ml final concentration) and analyzed on a FACSCanto machine (BD, Franklin Lakes, NJ, USA). Annexin V was prepared as previously described (Brumatti et al., Methods 2008). Viable cells are Annexin-V negative and PI negative, and cell death is expressed as 100% – viable cells.

Dynamic BH3 profiling

Dynamic BH3 profiling was performed as previously described in detail (Montero et al. Cancer Discovery 2017). ER+ breast cancer cell lines were incubated in RPMI with 10% FBS for MDA-MB-415 and T47D, and DMEM with 10% FBS for MCF7, at different times and drug concentration as indicated. To perform DBP in cell lines, 2×10^4 cells/well were used. We used a FACS-based BH3 profiling to perform the analysis, cytochrome c release was measured after a 60 minutes incubation of digitonin-permeabilized cells with BH3 peptides, as previously described (Ryan et al., Biol. Chem 2016).

Synergy scores

We quantify drug combination synergy using MuSyC (Meyer et al. 2019). MuSyC calculates the synergy score from drug combination kill curves and considers separately the effect of efficacy and potency. In this work, we focus on the synergy score of efficacy (β_{obs}). β_{obs} measures the percentage change in drug response of the drug combination when compared to that of each drug alone (at the highest concentration used for each drug alone and their combination). The synergy score of efficacy β_{obs} is such that $\beta_{obs} > 0$ means the drugs are synergistic, $\beta_{obs} < 0$ that they are antagonistic, and $\beta_{obs} = 0$ means the drugs show no synergistic or antagonistic effect.

Analysis of loss-of-function genetic screens, gene expression, and protein expression in cell line datasets

Analysis of the loss-of-function genetic screens from the Cancer Dependency Data (DepMap) and expression data from the Cancer Cell Line Encyclopedia (CCLE) followed a similar approach as in (Painter et al. 2020). Gene dependency data from CRISPR knockout (Avana data set), RNAi knockdown (Achilles and DRIVE data sets), gene expression (Ghandi et al. 2019) (RNA-seq from the CCLE), relative protein expression (Nusinow et al. 2020) (quantitative mass-spectroscopy proteomics from CCLE), and associated cell line annotations were taken from the DepMap 20Q1 Public data release (Dempster et al. 2019; DepMap 2020) (https://depmap.org/portal/download). Dependency for each gene and cell line is obtained using the CERES algorithm (Meyers et al. 2017) (for CRISPR knockout) or the DEMETER2 algorithm (McFarland et al. 2018) (for RNAi knockdown). Gene dependency is measured using the gene effect, which measures the impact of CRISPR knockout or RNAi knockdown of a gene on cell viability. The gene effect is normalized for each cell line so that a gene effect of 0 is the median dependency score of a negative control gene and a gene effect of -1 is the median dependency score of pan-essential genes (Dempster et al. 2019).

To infer the gene effect of MCL1 and p21 (*CDKN1A*) in T47D (a cell line not included in the DepMap CRISPR knockout screens), we use the gene effect of cell lines in which the gene of interest has a similar expression as in T47D. The inferred gene effect is defined as the median gene effect of cell lines within $\pm 2.5\%$of the $log_2\,(TPM+1)$ of T47D's expression of the gene of interest. In particular, we use *CDKN1A* expression to infer p21 gene effect and *BCL2L1* expression to infer MCL1 gene effect. This inference is based on the observation that the gene effect of MCL1 and the gene expression of *BCL2L1* are correlated across cell lines ($Pearson\ correlation = 0.45,\ p = 1.9\ \times 10^{-37}$;$Spearman\ correlation = 0.47,\ p = 7.2\ \times 10^{-41}$), and similarly for the gene effect of p21 and the gene expression of *CDKN1A* ($Pearson\ correlation = 0.48,\ p = 1.5\ \times 10^{-43}$;$Spearman\ correlation = 0.47, p = 2.4\ \times 10^{-41}$). For the case of MCL1, the inferred MCL1 gene effect is -0.40 ($median(gene\ effect) = -0.40$ for the 57 cell lines within $\pm 2.5\%$of the $log_2\,(TPM+1)$ of T47D's *BCL2L1* gene expression). For the case of p21, the inferred p21 gene effect is 0.17($median(gene\ effect) = 0.17$ for the 23 cell lines within $\pm 2.5\%$ of the $log_2\,(TPM+1)$ of T47D's *CDKN1A* gene expression).

Statistical analysis

All statistical analysis was performed using R (version 3.6.0). Pearson and Spearman correlations and p values were calculated using the *cor.test* function from the *stats* package using a two-sided test. Statistical comparisons in cell viability were performed using a two-sample, two-sided unpaired t-test using the *t.test* function from the *stats* package. A p value of less than 0.05 was considered to be statistically significant. Robust z-scores z for a value x_j in a distribution $D = [x_1, \ldots, x_n]$ were obtained by subtracting the median ($median$) and dividing by the median absolute deviation (mad), that is, $z(x_j) = [x_j - median(D)]/mad(D)$.

Dynamic network modeling

Our dynamic network modeling approach follows the methodology in (Gómez Tejeda Zañudo, Scaltriti, and Albert 2017), which uses a type of dynamic network model known as discrete dynamic network model. In a discrete dynamic network model, each node i in the directed network that underlies the model has an associated variable σ_i that can only take a discrete number of states. In the simplest case, the Boolean case, a node variable can only take the two states: 1 (active) or 0 (inactive). The state of a variable σ_i is determined using a regulatory function f_i, which depends on the variable of a node j only if there is a directed interaction from j to i ($j \rightarrow i$).

The state of the system $\Sigma(t) = [\sigma_1(t),\ \sigma_2(t), \ldots, \sigma_N(t)]$, where $\sigma_i(t)$ is the state of variable σ_i at time t, changes in time following a general asynchronous updating scheme (Garg et al. 2008; Saadatpour, Albert, and Albert 2010). In general asynchronous updating, the state of the system is updated in discrete time units by (1) choosing one randomly selected node k at each time step t (with update probability p_k) and updating its state based on the state of the system at the previous time step ($\sigma_k(t) = f_k(\Sigma(t-1))$ and (2) transferring the node state from the previous time step of the rest of the nodes ($\sigma_l(t) = \sigma_l(t-1),\ l \neq k$).

Model simulations

Model simulations were performed using similar methodology as in (Gómez Tejeda Zañudo, Scaltriti, and Albert 2017). The simulations of the discrete network models were done by mapping the discrete network model into a Boolean model, which was then simulated using the BooleanDynamicModeling Java library, which is available on GitHub (https://github.com/jgtz/BooleanDynamicModeling). To simulate multi-level nodes, we use a Boolean variable to denote each level greater than 1. For example, for a 3-level node with states 0, 1, and 2, we have 2 variables (Node and Node_2), and for a 4-level node we have 3 variables (Node, Node_2, and Node_3). The updating probabilities are chosen by categorizing nodes into either a fast or slow node,

according to whether activation of the node denotes a (fast) signaling event or a (slow) transcriptional or translational event. The regulatory functions of all the nodes are indicated and explained in Supplemental Text and Supplemental File 1. We perform 10,000 simulations in each modeled scenario. The number of time units is 25 for all simulations, where a time unit is equal to the average number of time steps needed to update a slow node. More details on the network model and the model simulations can be found in the Supplemental Text and Supplemental File 1.

The code used to simulate the model is available on GitHub (https://github.com/jgtz/BreastCancerModelv2), and includes a Jupyter notebook that generates all the model results. To allow easy reuse of the model, we use bioLQM (Naldi 2018) (version 0.6.1, https://github.com/colomoto/bioLQM) to make the model available in Systems Biology Markup Language (SBML) format on the GitHub repository.

List of Supplemental Material

Supplemental File 1

Supplemental Text

Supplemental Figures S1-S6

References

Alberghina, Lilia, and Hans V. Westerhoff. 2007. *Systems Biology: Definitions and Perspectives*. Springer Science & Business Media.

André, Fabrice, Eva Ciruelos, Gabor Rubovszky, Mario Campone, Sibylle Loibl, Hope S. Rugo, Hiroji Iwata, et al. 2019. “Alpelisib for PIK3CA-Mutated, Hormone Receptor–Positive Advanced Breast Cancer.” *The New England Journal of Medicine* 380 (20): 1929–40.

Barrette, Anne Marie, Mehdi Bouhaddou, and Marc R. Birtwistle. 2018. “Integrating Transcriptomic Data with Mechanistic Systems Pharmacology Models for Virtual Drug Combination Trials.” *ACS Chemical Neuroscience* 9 (1): 118–29.

Béal, Jonas, Arnau Montagud, Pauline Traynard, Emmanuel Barillot, and Laurence Calzone. 2018. “Personalization of Logical Models With Multi-Omics Data Allows Clinical Stratification of Patients.” *Frontiers in Physiology* 9: 1965.

Bertoli, Cosetta, and Robertus Antonius Maria de Bruin. 2014. “Cell Division: Turning Cell Cycle Entry on Its Head.” *eLife* 3: e03475.

Bertucci, François, Charlotte K. Y. Ng, Anne Patsouris, Nathalie Droin, Salvatore Piscuoglio, Nadine Carbuccia, Jean Charles Soria, et al. 2019. “Author Correction: Genomic Characterization of Metastatic Breast Cancers.” *Nature* 572 (7767): E7.

Bhola, Patrick D., Eman Ahmed, Jennifer L. Guerriero, Ewa Sicinska, Emily Su, Elizaveta Lavrova, Jing Ni, et al. 2020. “High-Throughput Dynamic BH3 Profiling May Quickly and Accurately Predict Effective Therapies in Solid Tumors.” *Science Signaling* 13 (636). https://doi.org/10.1126/scisignal.aay1451.

Bosch, Ana, Zhiqiang Li, Anna Bergamaschi, Haley Ellis, Eneda Toska, Aleix Prat, Jessica J. Tao, et al. 2015. “PI3K Inhibition Results in Enhanced Estrogen Receptor Function and Dependence in Hormone Receptor–positive Breast Cancer.” *Science Translational Medicine* 7 (283): 283ra51–283ra51.

Brady, Renee, and Heiko Enderling. 2019. “Mathematical Models of Cancer: When to Predict Novel Therapies, and When Not to.” *Bulletin of Mathematical Biology* 81 (10): 3722–31.

Brunet, A., A. Bonni, M. J. Zigmond, M. Z. Lin, P. Juo, L. S. Hu, M. J. Anderson, K. C. Arden, J. Blenis, and M. E. Greenberg. 1999. “Akt Promotes Cell Survival by Phosphorylating and Inhibiting a Forkhead Transcription Factor.” *Cell* 96 (6): 857–68.

Castel, Pau, Haley Ellis, Ruzica Bago, Eneda Toska, Pedram Razavi, F. Javier Carmona, Srinivasaraghavan Kannan, et al. 2016. “PDK1-SGK1 Signaling Sustains AKT-Independent mTORC1 Activation and Confers Resistance to PI3Kα Inhibition.” *Cancer Cell* 30 (2): 229–42.

Caswell-Jin, Jennifer L., Sylvia K. Plevritis, Lu Tian, Christopher J. Cadham, Cong Xu, Natasha K. Stout, George W. Sledge, Jeanne S. Mandelblatt, and Allison W. Kurian. 2018. “Change in Survival in Metastatic Breast Cancer with Treatment Advances: Meta-Analysis and Systematic Review.” *JNCI Cancer Spectrum* 2 (4): ky062.

Chandarlapaty, Sarat, Ayana Sawai, Maurizio Scaltriti, Vanessa Rodrik-Outmezguine, Olivera Grbovic-Huezo, Violeta Serra, Pradip K. Majumder, Jose Baselga, and Neal Rosen. 2011. “AKT Inhibition Relieves Feedback Suppression of Receptor Tyrosine Kinase Expression and Activity.” *Cancer Cell* 19 (1): 58–71.

Clarke, Matthew A., and Jasmin Fisher. 2020. “Executable Cancer Models: Successes and Challenges.” *Nature Reviews. Cancer* 20 (6): 343–54.

Costa, Carlotta, Hiromichi Ebi, Miriam Martini, Sean A. Beausoleil, Anthony C. Faber, Charles T. Jakubik, Alan Huang, et al. 2015. “Measurement of PIP3 Levels Reveals an Unexpected Role for p110β in Early Adaptive Responses to p110α-Specific Inhibitors in Luminal Breast Cancer.” *Cancer Cell* 27 (1): 97–108.

Costa, Carlotta, Ye Wang, Amy Ly, Yasuyuki Hosono, Ellen Murchie, Charlotte S. Walmsley, Tiffany Huynh, et al. 2020. “PTEN Loss Mediates Clinical Cross-Resistance to CDK4/6 and PI3Kα Inhibitors in Breast Cancer.” *Cancer Discovery* 10 (1): 72–85.

Coutant, Anthony, Katherine Roper, Daniel Trejo-Banos, Dominique Bouthinon, Martin Carpenter, Jacek Grzebyta, Guillaume Santini, et al. 2019. “Closed-Loop Cycles of Experiment Design, Execution, and Learning Accelerate Systems Biology Model Development in Yeast.” *Proceedings of the National Academy of Sciences of the United States of America* 116 (36): 18142–47.

Dempster, Joshua M., Jordan Rossen, Mariya Kazachkova, Joshua Pan, Guillaume Kugener, David E. Root, and Aviad Tsherniak. 2019. “Extracting Biological Insights from the Project Achilles Genome-Scale CRISPR Screens in Cancer Cell Lines.” *bioRxiv*. https://doi.org/10.1101/720243.

DepMap, Broad. 2020. “DepMap 20Q1 Public.” https://doi.org/10.6084/m9.figshare.11791698.v3.

Donnella, Hayley J., James T. Webber, Rebecca S. Levin, Roman Camarda, Olga Momcilovic, Nora Bayani, Khyati N. Shah, et al. 2018. “Kinome Rewiring Reveals AURKA Limits PI3K-Pathway Inhibitor Efficacy in Breast Cancer.” *Nature Chemical Biology* 14 (8): 768–77.

Elkabets, Moshe, Sadhna Vora, Dejan Juric, Natasha Morse, Mari Mino-Kenudson, Taru Muranen, Jessica Tao, et al. 2013. “mTORC1 Inhibition Is Required for Sensitivity to PI3K p110α Inhibitors in PIK3CA-Mutant Breast Cancer.” *Science Translational Medicine* 5 (196): 196ra99.

Ezhevsky, S. A., H. Nagahara, A. M. Vocero-Akbani, D. R. Gius, M. C. Wei, and S. F. Dowdy. 1997. “Hypo-Phosphorylation of the Retinoblastoma Protein (pRb) by Cyclin D:Cdk4/6 Complexes Results in Active pRb.” *Proceedings of the National Academy of Sciences of the United States of America* 94 (20): 10699–704.

Fey, Dirk, Melinda Halasz, Daniel Dreidax, Sean P. Kennedy, Jordan F. Hastings, Nora Rauch, Amaya Garcia Munoz, et al. 2015. “Signaling Pathway Models as Biomarkers: Patient-Specific Simulations of JNK Activity Predict the Survival of Neuroblastoma Patients.” *Science Signaling* 8 (408): ra130.

Fröhlich, Fabian, Thomas Kessler, Daniel Weindl, Alexey Shadrin, Leonard Schmiester, Hendrik Hache, Artur Muradyan, et al. 2018. “Efficient Parameter Estimation Enables the Prediction of Drug Response Using a Mechanistic Pan-Cancer Pathway Model.” *Cell Systems* 7 (6): 567–79.e6.

Garg, Abhishek, Alessandro Di Cara, Ioannis Xenarios, Luis Mendoza, and Giovanni De Micheli. 2008. “Synchronous versus Asynchronous Modeling of Gene Regulatory Networks.” *Bioinformatics* 24 (17): 1917–25.

Ghandi, Mahmoud, Franklin W. Huang, Judit Jané-Valbuena, Gregory V. Kryukov, Christopher C. Lo, E. Robert McDonald 3rd, Jordi Barretina, et al. 2019. “Next-Generation Characterization of the Cancer Cell Line Encyclopedia.” *Nature* 569 (7757): 503–8.

Gómez Tejeda Zañudo, Jorge, Maurizio Scaltriti, and Réka Albert. 2017. “A Network Modeling Approach to Elucidate Drug Resistance Mechanisms and Predict Combinatorial Drug Treatments in Breast Cancer.” *Cancer Convergence* 1 (1): 5.

G. T. Zañudo, Jorge, Steven N. Steinway, and Réka Albert. 2018. “Discrete Dynamic Network Modeling of Oncogenic Signaling: Mechanistic Insights for Personalized Treatment of Cancer.” *Current Opinion in Systems Biology* 9 (June): 1–10.

Herrera-Abreu, Maria Teresa, Marta Palafox, Uzma Asghar, Martín A. Rivas, Rosalind J. Cutts, Isaac Garcia-

Murillas, Alex Pearson, et al. 2016. “Early Adaptation and Acquired Resistance to CDK4/6 Inhibition in Estrogen Receptor-Positive Breast Cancer.” *Cancer Research* 76 (8): 2301–13.
Hopkins, Benjamin D., Chantal Pauli, Xing Du, Diana G. Wang, Xiang Li, David Wu, Solomon C. Amadiume, et al. 2018. “Suppression of Insulin Feedback Enhances the Efficacy of PI3K Inhibitors.” *Nature* 560 (7719): 499–503.
Hu, Mickey C-T, Dung-Fang Lee, Weiya Xia, Leonard S. Golfman, Fu Ou-Yang, Jer-Yen Yang, Yiyu Zou, et al. 2004. “IκB Kinase Promotes Tumorigenesis through Inhibition of Forkhead FOXO3a.” *Cell* 117 (2): 225–37.
Ilic, Nina, Tamara Utermark, Hans R. Widlund, and Thomas M. Roberts. 2011. “PI3K-Targeted Therapy Can Be Evaded by Gene Amplification along the MYC-Eukaryotic Translation Initiation Factor 4E (eIF4E) Axis.” *Proceedings of the National Academy of Sciences of the United States of America* 108 (37): E699–708.
Juric, Dejan, Pau Castel, Malachi Griffith, Obi L. Griffith, Helen H. Won, Haley Ellis, Saya H. Ebbesen, et al. 2015. “Convergent Loss of PTEN Leads to Clinical Resistance to a PI(3)Kα Inhibitor.” *Nature* 518 (7538): 240–44.
Kodack, David P., Vasileios Askoxylakis, Gino B. Ferraro, Qing Sheng, Mark Badeaux, Shom Goel, Xiaolong Qi, et al. 2017. “The Brain Microenvironment Mediates Resistance in Luminal Breast Cancer to PI3K Inhibition through HER3 Activation.” *Science Translational Medicine* 9 (391). https://doi.org/10.1126/scitranslmed.aal4682.
Konieczkowski, David J., Cory M. Johannessen, and Levi A. Garraway. 2018. “A Convergence-Based Framework for Cancer Drug Resistance.” *Cancer Cell* 33 (5): 801–15.
Kotschy, András, Zoltán Szlavik, James Murray, James Davidson, Ana Leticia Maragno, Gaëtane Le Toumelin-Braizat, Maïa Chanrion, et al. 2016. “The MCL1 Inhibitor S63845 Is Tolerable and Effective in Diverse Cancer Models.” *Nature* 538 (7626): 477–82.
Le, Xiuning, Rajee Antony, Pedram Razavi, Daniel J. Treacy, Flora Luo, Mahmoud Ghandi, Pau Castel, Maurizio Scaltriti, Jose Baselga, and Levi A. Garraway. 2016. “Systematic Functional Characterization of Resistance to PI3K Inhibition in Breast Cancer.” *Cancer Discovery* 6 (10): 1134–47.
Liang, Jiyong, Judit Zubovitz, Teresa Petrocelli, Rouslan Kotchetkov, Michael K. Connor, Kathy Han, Jin-Hwa Lee, et al. 2002. “PKB/Akt Phosphorylates p27, Impairs Nuclear Import of p27 and Opposes p27-Mediated G1 Arrest.” *Nature Medicine* 8 (10): 1153–60.
Liberzon, Arthur, Chet Birger, Helga Thorvaldsdóttir, Mahmoud Ghandi, Jill P. Mesirov, and Pablo Tamayo. 2015. “The Molecular Signatures Database (MSigDB) Hallmark Gene Set Collection.” *Cell Systems* 1 (6): 417–25.
Lito, Piro, Neal Rosen, and David B. Solit. 2013. “Tumor Adaptation and Resistance to RAF Inhibitors.” *Nature Medicine* 19 (11): 1401–9.
Lok, S. W., J. R. Whittle, F. Vaillant, C. E. Teh, and L. L. Lo. 2019. “A Phase Ib Dose-Escalation and Expansion Study of the BCL2 Inhibitor Venetoclax Combined with Tamoxifen in ER and BCL2–positive Metastatic Breast Cancer.” *Cancer Discovery*. https://cancerdiscovery.aacrjournals.org/content/9/3/354.abstract.
Lundberg, A. S., and R. A. Weinberg. 1998. “Functional Inactivation of the Retinoblastoma Protein Requires Sequential Modification by at Least Two Distinct Cyclin-Cdk Complexes.” *Molecular and Cellular Biology* 18 (2): 753–61.
Ma, Xiaoju Max, and John Blenis. 2009. “Molecular Mechanisms of mTOR-Mediated Translational Control.” *Nature Reviews. Molecular Cell Biology* 10 (5): 307–18.
McFarland, James M., Zandra V. Ho, Guillaume Kugener, Joshua M. Dempster, Phillip G. Montgomery, Jordan G. Bryan, John M. Krill-Burger, et al. 2018. “Improved Estimation of Cancer Dependencies from Large-Scale RNAi Screens Using Model-Based Normalization and Data Integration.” *Nature Communications* 9 (1): 4610.
Medema, R. H., G. J. Kops, J. L. Bos, and B. M. Burgering. 2000. “AFX-like Forkhead Transcription Factors Mediate Cell-Cycle Regulation by Ras and PKB through p27kip1.” *Nature* 404 (6779): 782–87.
Meyer, Christian T., David J. Wooten, B. Bishal Paudel, Joshua Bauer, Keisha N. Hardeman, David Westover, Christine M. Lovly, Leonard A. Harris, Darren R. Tyson, and Vito Quaranta. 2019. “Quantifying Drug Combination Synergy along Potency and Efficacy Axes.” *Cell Systems* 8 (2): 97–108.e16.
Meyers, Robin M., Jordan G. Bryan, James M. McFarland, Barbara A. Weir, Ann E. Sizemore, Han Xu, Neekesh V. Dharia, et al. 2017. “Computational Correction of Copy Number Effect Improves Specificity of CRISPR-Cas9 Essentiality Screens in Cancer Cells.” *Nature Genetics* 49 (12): 1779–84.

Montero, Joan, Kristopher A. Sarosiek, Joseph D. DeAngelo, Ophélia Maertens, Jeremy Ryan, Dalia Ercan, Huiying Piao, et al. 2015. “Drug-Induced Death Signaling Strategy Rapidly Predicts Cancer Response to Chemotherapy.” *Cell* 160 (5): 977–89.

Montero, Joan, Cécile Gstalder, Daniel J. Kim, Dorota Sadowicz, Wayne Miles, Michael Manos, Justin R. Cidado et al. 2019. "Destabilization of NOXA mRNA as a common resistance mechanism to targeted therapies." *Nature communications* 10 (1): 1-15.

Muellner, Markus K., Iris Z. Uras, Bianca V. Gapp, Claudia Kerzendorfer, Michal Smida, Hannelore Lechtermann, Nils Craig-Mueller, Jacques Colinge, Gerhard Duernberger, and Sebastian M. B. Nijman. 2011. “A Chemical-Genetic Screen Reveals a Mechanism of Resistance to PI3K Inhibitors in Cancer.” *Nature Chemical Biology* 7 (11): 787–93.

Muranen, Taru, Laura M. Selfors, Devin T. Worster, Marcin P. Iwanicki, Loling Song, Fabiana C. Morales, Sizhen Gao, Gordon B. Mills, and Joan S. Brugge. 2012. “Inhibition of PI3K/mTOR Leads to Adaptive Resistance in Matrix-Attached Cancer Cells.” *Cancer Cell* 21 (2): 227–39.

Naldi, Aurélien. 2018. “BioLQM: A Java Toolkit for the Manipulation and Conversion of Logical Qualitative Models of Biological Networks.” *Frontiers in Physiology* 9 (November): 1605.

Ni Chonghaile, Triona, Kristopher A. Sarosiek, Thanh-Trang Vo, Jeremy A. Ryan, Anupama Tammareddi, Victoria Del Gaizo Moore, Jing Deng, et al. 2011. “Pretreatment Mitochondrial Priming Correlates with Clinical Response to Cytotoxic Chemotherapy.” *Science* 334 (6059): 1129–33.

Nusinow, David P., John Szpyt, Mahmoud Ghandi, Christopher M. Rose, E. Robert McDonald 3rd, Marian Kalocsay, Judit Jané-Valbuena, et al. 2020. “Quantitative Proteomics of the Cancer Cell Line Encyclopedia.” *Cell* 180 (2): 387–402.e16.

Painter, Corrie A., Esha Jain, Brett N. Tomson, Michael Dunphy, Rachel E. Stoddard, Beena S. Thomas, Alyssa L. Damon, et al. 2020. “The Angiosarcoma Project: Enabling Genomic and Clinical Discoveries in a Rare Cancer through Patient-Partnered Research.” *Nature Medicine* 26 (2): 181–87.

Planas-Silva, M. D., and R. A. Weinberg. 1997. “Estrogen-Dependent Cyclin E-cdk2 Activation through p21 Redistribution.” *Molecular and Cellular Biology* 17 (7): 4059–69.

Polyak, K., M. H. Lee, H. Erdjument-Bromage, A. Koff, J. M. Roberts, P. Tempst, and J. Massagué. 1994. “Cloning of p27Kip1, a Cyclin-Dependent Kinase Inhibitor and a Potential Mediator of Extracellular Antimitogenic Signals.” *Cell* 78 (1): 59–66.

Razavi, Pedram, Matthew T. Chang, Guotai Xu, Chaitanya Bandlamudi, Dara S. Ross, Neil Vasan, Yanyan Cai, et al. 2018. “The Genomic Landscape of Endocrine-Resistant Advanced Breast Cancers.” *Cancer Cell* 34 (3): 427–38.e6.

Razavi, Pedram, Maura N. Dickler, Payal D. Shah, Weiyi Toy, David N. Brown, Helen H. Won, Bob T. Li, et al. 2020. “Alterations in PTEN and ESR1 Promote Clinical Resistance to Alpelisib plus Aromatase Inhibitors.” *Nature Cancer* 1 (4): 382–93.

Rockne, Russell C., Andrea Hawkins-Daarud, Kristin R. Swanson, James P. Sluka, James A. Glazier, Paul Macklin, David A. Hormuth, et al. 2019. “The 2019 Mathematical Oncology Roadmap.” *Physical Biology* 16 (4): 041005.

Saadatpour, Assieh, István Albert, and Réka Albert. 2010. “Attractor Analysis of Asynchronous Boolean Models of Signal Transduction Networks.” *Journal of Theoretical Biology* 266 (4): 641–56.

Saez-Rodriguez, Julio, and Nils Blüthgen. 2020. “Personalized Signaling Models for Personalized Treatments.” *Molecular Systems Biology* 16 (1): e9042.

Schaub, Franz X., Varsha Dhankani, Ashton C. Berger, Mihir Trivedi, Anne B. Richardson, Reid Shaw, Wei Zhao, et al. 2018. “Pan-Cancer Alterations of the MYC Oncogene and Its Proximal Network across the Cancer Genome Atlas.” *Cell Systems* 6 (3): 282–300.e2.

Schwartz, Sarit, John Wongvipat, Cath B. Trigwell, Urs Hancox, Brett S. Carver, Vanessa Rodrik-Outmezguine, Marie Will, et al. 2015. “Feedback Suppression of PI3Kα Signaling in PTEN-Mutated Tumors Is Relieved by Selective Inhibition of PI3Kβ.” *Cancer Cell* 27 (1): 109–22.

Sherr, C. J., and J. M. Roberts. 1999. “CDK Inhibitors: Positive and Negative Regulators of G1-Phase Progression.” *Genes & Development* 13 (12): 1501–12.

Steeg, Patricia S. 2016. “Targeting Metastasis.” *Nature Reviews. Cancer* 16 (4): 201–18.

Steinway, Steven Nathaniel, Jorge Gomez Tejeda Zañudo, Paul J. Michel, David J. Feith, Thomas P. Loughran, and Reka Albert. 2015. “Combinatorial Interventions Inhibit TGFβ-Driven Epithelial-to-Mesenchymal Transition and Support Hybrid Cellular Phenotypes.” *NPJ Systems Biology and Applications* 1 (November): 15014.

Sun, Chong, and René Bernards. 2014. “Feedback and Redundancy in Receptor Tyrosine Kinase Signaling: Relevance to Cancer Therapies.” *Trends in Biochemical Sciences* 39 (10): 465–74.

Toska, Eneda, Hatice U. Osmanbeyoglu, Pau Castel, Carmen Chan, Ronald C. Hendrickson, Moshe Elkabets, Maura N. Dickler, et al. 2017. “PI3K Pathway Regulates ER-Dependent Transcription in Breast Cancer through the Epigenetic Regulator KMT2D.” *Science* 355 (6331): 1324–30.

Vasan, Neil, José Baselga, and David M. Hyman. 2019. “A View on Drug Resistance in Cancer.” *Nature* 575 (7782): 299–309.

Viglietto, Giuseppe, Maria Letizia Motti, Paola Bruni, Rosa Marina Melillo, Amelia D’Alessio, Daniela Califano, Floriana Vinci, et al. 2002. “Cytoplasmic Relocalization and Inhibition of the Cyclin-Dependent Kinase Inhibitor p27(Kip1) by PKB/Akt-Mediated Phosphorylation in Breast Cancer.” *Nature Medicine* 8 (10): 1136–44.

Vora, Sadhna R., Dejan Juric, Nayoon Kim, Mari Mino-Kenudson, Tiffany Huynh, Carlotta Costa, Elizabeth L. Lockerman, et al. 2014. “CDK 4/6 Inhibitors Sensitize PIK3CA Mutant Breast Cancer to PI3K Inhibitors.” *Cancer Cell* 26 (1): 136–49.

Waks, Adrienne G., and Eric P. Winer. 2019. “Breast Cancer Treatment: A Review.” *JAMA: The Journal of the American Medical Association* 321 (3): 288–300.

Wander, Seth A., Ofir Cohen, Xueqian Gong, Gabriela N. Johnson, Jorge E. Buendia-Buendia, Maxwell R. Lloyd, Dewey Kim, et al. 2020. “The Genomic Landscape of Intrinsic and Acquired Resistance to Cyclin-Dependent Kinase 4/6 Inhibitors in Patients with Hormone Receptor Positive Metastatic Breast Cancer.” *Cancer Discovery*, May. https://doi.org/10.1158/2159-8290.CD-19-1390.

Wander, Seth A., Dekuang Zhao, and Joyce M. Slingerland. 2011. “p27: A Barometer of Signaling Deregulation and Potential Predictor of Response to Targeted Therapies.” *Clinical Cancer Research: An Official Journal of the American Association for Cancer Research* 17 (1): 12–18.

Weigelt, Britta, Johannes L. Peterse, and Laura J. van ’t Veer. 2005. “Breast Cancer Metastasis: Markers and Models.” *Nature Reviews. Cancer* 5 (8): 591–602.

Whittle, James R., François Vaillant, Elliot Surgenor, Antonia N. Policheni, Göknur Giner, Bianca D. Capaldo, Huei-Rong Chen, et al. 2020. “Dual Targeting of CDK4/6 and BCL2 Pathways Augments Tumor Response in Estrogen Receptor-Positive Breast Cancer.” *Clinical Cancer Research: An Official Journal of the American Association for Cancer Research*, April. https://doi.org/10.1158/1078-0432.CCR-19-1872.

Wooten, D. J., C. T. Meyer, V. Quaranta, and C. F. Lopez. 2019. “A Consensus Framework Unifies Multi-Drug Synergy Metrics.” *bioRxiv*. https://www.biorxiv.org/content/10.1101/683433v1.abstract.

Zhang, Xinbo, Naimei Tang, Timothy J. Hadden, and Arun K. Rishi. 2011. “Akt, FoxO and Regulation of Apoptosis.” *Biochimica et Biophysica Acta* 1813 (11): 1978–86.

Zhang, Yiqun, Patrick Kwok-Shing Ng, Melanie Kucherlapati, Fengju Chen, Yuexin Liu, Yiu Huen Tsang, Guillermo de Velasco, et al. 2017. “A Pan-Cancer Proteogenomic Atlas of PI3K/AKT/mTOR Pathway Alterations.” *Cancer Cell* 31 (6): 820–32.e3.

Zhou, B. P., Y. Liao, W. Xia, B. Spohn, M. H. Lee, and M. C. Hung. 2001. “Cytoplasmic Localization of p21Cip1/WAF1 by Akt-Induced Phosphorylation in HER-2/neu-Overexpressing Cells.” *Nature Cell Biology* 3 (3): 245–52.

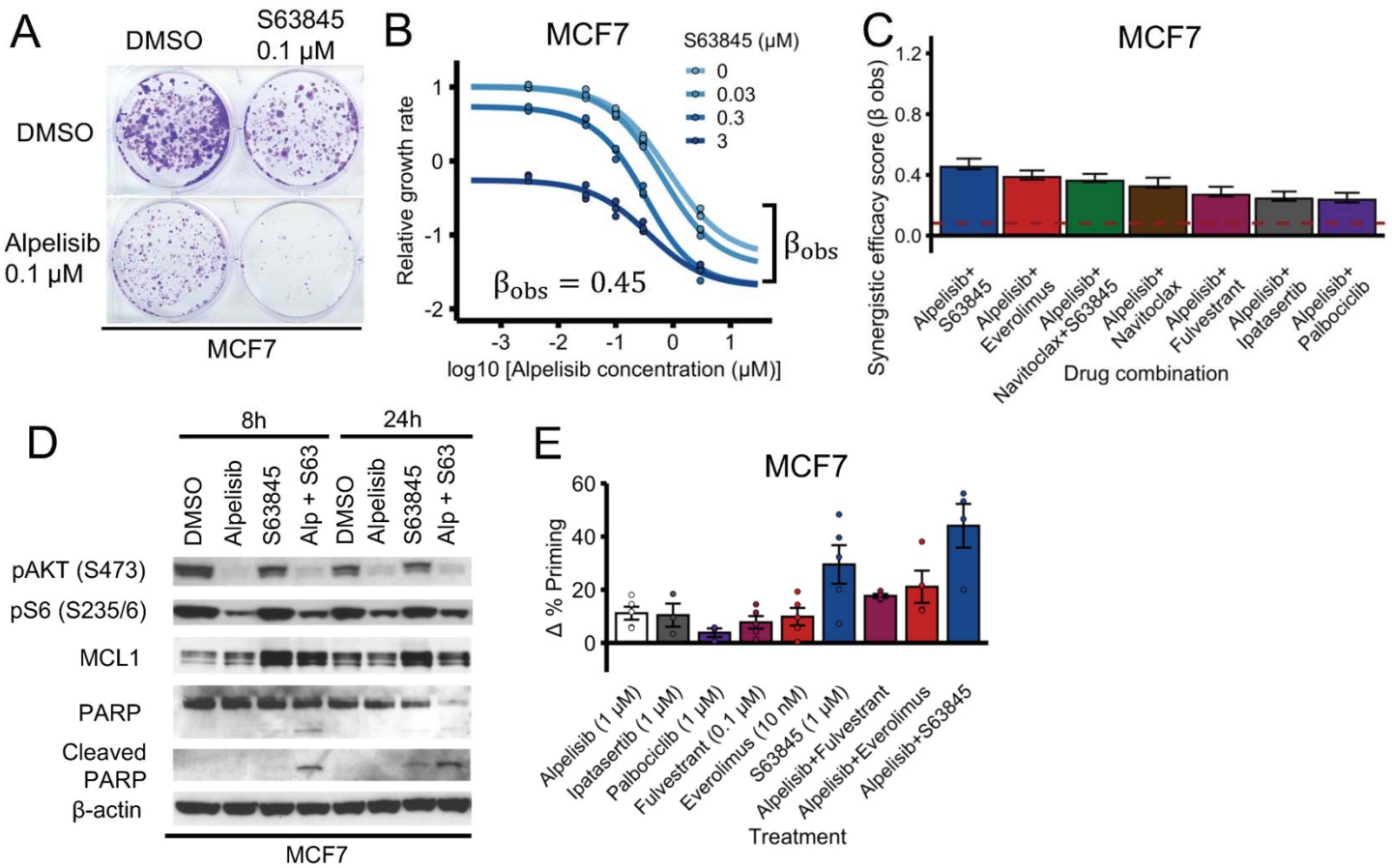

Fig. 1. PI3Kα inhibitors and MCL1 inhibitors are a synergistically efficacious combination and induce apoptosis in MCF7. (A, B) PI3Kα inhibitor Alpelisib and MCL1 inhibitor S63845 is an effective and synergistically efficacious drug combination. MCF7 cells were treated with Alpelisib, S63845, and their combination. For panel A, cells a colony formation assay was performed after 18 days of drug treatment. For panel B, CellTiter-Glo assay was performed before drug treatment and after 6 days of drug treatment to measure cell viability. The relative growth rate is calculated with respect to the DMSO control treatment using cell viability. Efficacy scores β_{obs} are such that $\beta_{obs} > 0$ means synergistic behavior and $\beta_{obs} < 0$ means antagonistic behavior, and are calculated using MuSyC (Meyer et al. 2019). (C) The combination of Alpelisib and S63845 is equally synergistically efficacious (or more) than clinically relevant drugs like Fulvestrant, Everolimus, and Palbociclib. The dotted red line ($\beta_{obs} = 0.08$) is the null-hypothesis synergy score value expected from doubling the Alpelisib combination (i.e., a combination of Alpelisib with itself). Experiments were done and synergy scores β_{obs} were calculated as in panel B. (D) Combined Alpelisib and S63845 result in an increase in apoptosis (as measured by cleaved PARP levels) compared to each separate drug. Consistent with the known effects of Alpelisib and S63845, we observe that Alpelisib (0.1 μM) decreased phosphorylation of AKT (S473) and S6 (S235/6) (downstream targets of PI3K signaling), and that S63845 (0.1 μM) increased MCL1 protein levels (due to S63845's binding to MCL1, which results in its inhibition (Kotschy et al. 2016)). (E) The combination of Alpelisib with S63845 results in an increased apoptosis priming compared to the combination with clinically relevant drugs like Fulvestrant and Everolimus. Δ% apoptosis priming for a treatment was measured using dynamic BH3 profiling by comparing treated vs untreated cells after 16 h under increased concentration of BIM peptide.

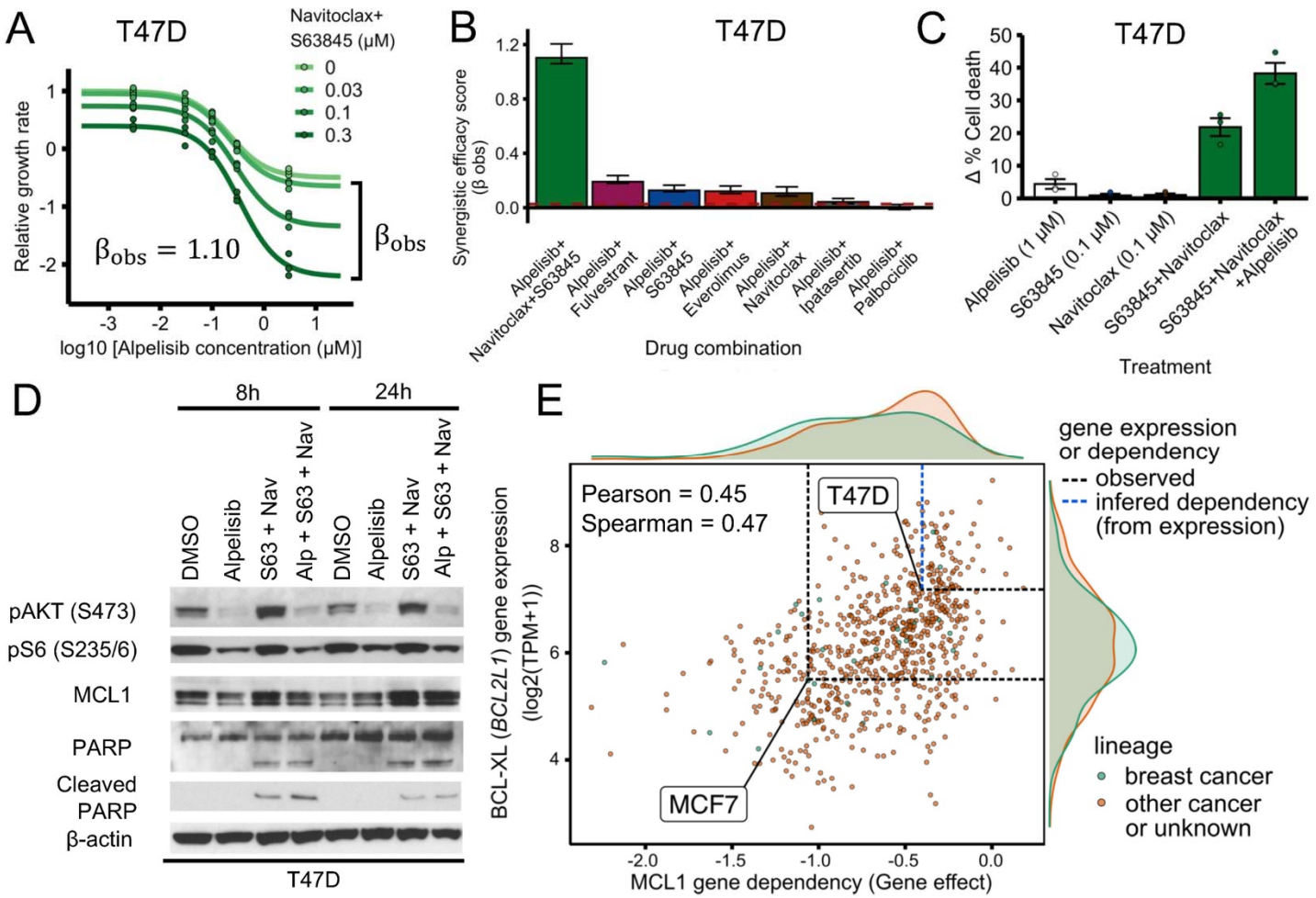

Fig. 2. PI3Kα inhibitors and BH3 mimetics are a synergistically efficacious combination and induce apoptosis in T47D. (A) PI3Kα inhibitor Alpelisib, MCL1 inhibitor S63845, and BCL-2/BCL-XL inhibitor Navitoclax is an effective and synergistically efficacious drug combination. T47D cells were treated with Alpelisib, S63845 and Navitoclax (1 μM), and their combination. CellTiter-Glo assay was performed before drug treatment and after 6 days of drug treatment to measure cell viability. The relative growth rate is calculated with respect to the DMSO control treatment using cell viability. Efficacy scores β_{obs} are such that $\beta_{obs} > 0$ means synergistic behavior and $\beta_{obs} < 0$ means antagonistic behavior, and are calculated using MuSyC (Meyer et al. 2019). (B) The combination of Alpelisib, S63845, and Navitoclax is more synergistically efficacious than clinically relevant drugs like Fulvestrant, Everolimus, and Palbociclib. The dotted red line ($\beta_{obs} = 0.03$) is the null-hypothesis synergy score value expected from doubling the Alpelisib combination (i.e., a combination of Alpelisib with itself). Experiments were done and synergy scores β_{obs} were calculated as in Fig. 1. (C, D) Combined Alpelisib, S63845, and Navitoclax result in an increase in apoptosis compared to each separate drug. Apoptosis was measured using annexin V (panel C) and cleaved PARP levels (panel D). Δ% cell death for a treatment was measured using annexin V by comparing treated vs DMSO control cells after 72 h (panel C). The decreased phosphorylation of AKT (S473) and S6 (S235/6), and increased levels of MCL1 are consistent with the known effects of Alpelisib and S63845 (see Fig. 1). Drug concentrations used were: 0.1 μM for Alpelisib, 0.3 μM for S63845, and 0.3 μM for Navitoclax (panel D). (E) Sensitivity to MCL1 knockout in CRISPR/Cas-9 loss-of-function screens (DepMap) is strongly correlated with BCL-XL gene expression. Based on T47D's BCL-XL gene expression, T47D is inferred to be less sensitive to MCL1 knockout than MCF7, consistent with T47D requiring Navitoclax to be sensitive to combined Alpelisib and S63845. Sensitivity to gene knockout is measured using gene effect, which is such that gene effect=0 means no effect and gene effect=-1 is the median effect of known common essential genes. Inferred gene effect is shown with a dashed blue line; gene expression or gene effect from the dataset is shown with a dashed black line.

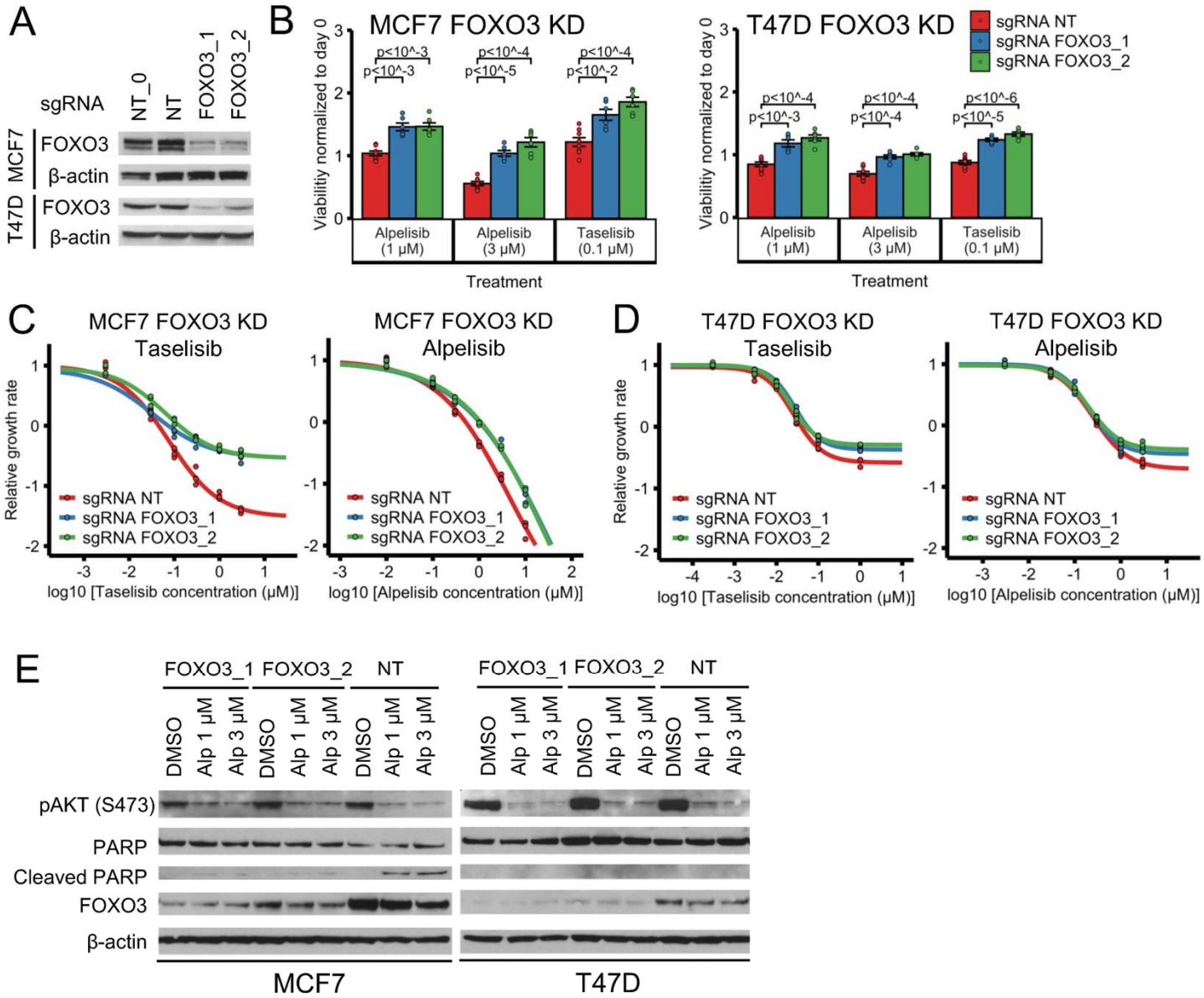

Fig. 3. FOXO3 knockdown reduces sensitivity to PI3Kα inhibitors in ER+ breast cancer cell line models. (A) Stable cell lines generated using CRISPR FOXO3 knockdown have with reduced proteins levels of FOXO3. NT and NT_0 are two distinct non-targeting control guides; FOXO3_1 and FOXO3_2 are two distinct guides targeting FOXO3. (B-D) FOXO3 knockdown reduces sensitivity to PI3Kα inhibitors Alpelisib and Taselisib in ER+ breast cancer cell lines MCF7 and T47D. CellTiter-Glo assay was used to measure cell viability before drug treatment and after 6 days of drug treatment. An unpaired, two-sided t-test was used for comparison between groups (panel B). Experiments in panel B single-dose experiments were optimized for the tested PI3Kα inhibitor concentrations: panel B used a larger number of initial cells than panels C and D (5,000 vs 1,000 cells), and measure the viability with respect to the cells before treatment. Panels C and D calculate the relative growth rate with respect to DMSO control. (E) FOXO3 knockdown reduces PI3Kα-inhibitor-induced cell death in MCF7. Cell death was measured using cleaved PARP levels. The decreased phosphorylation of AKT (S473) is consistent with the known downregulation of PI3K signaling by Alpelisib.

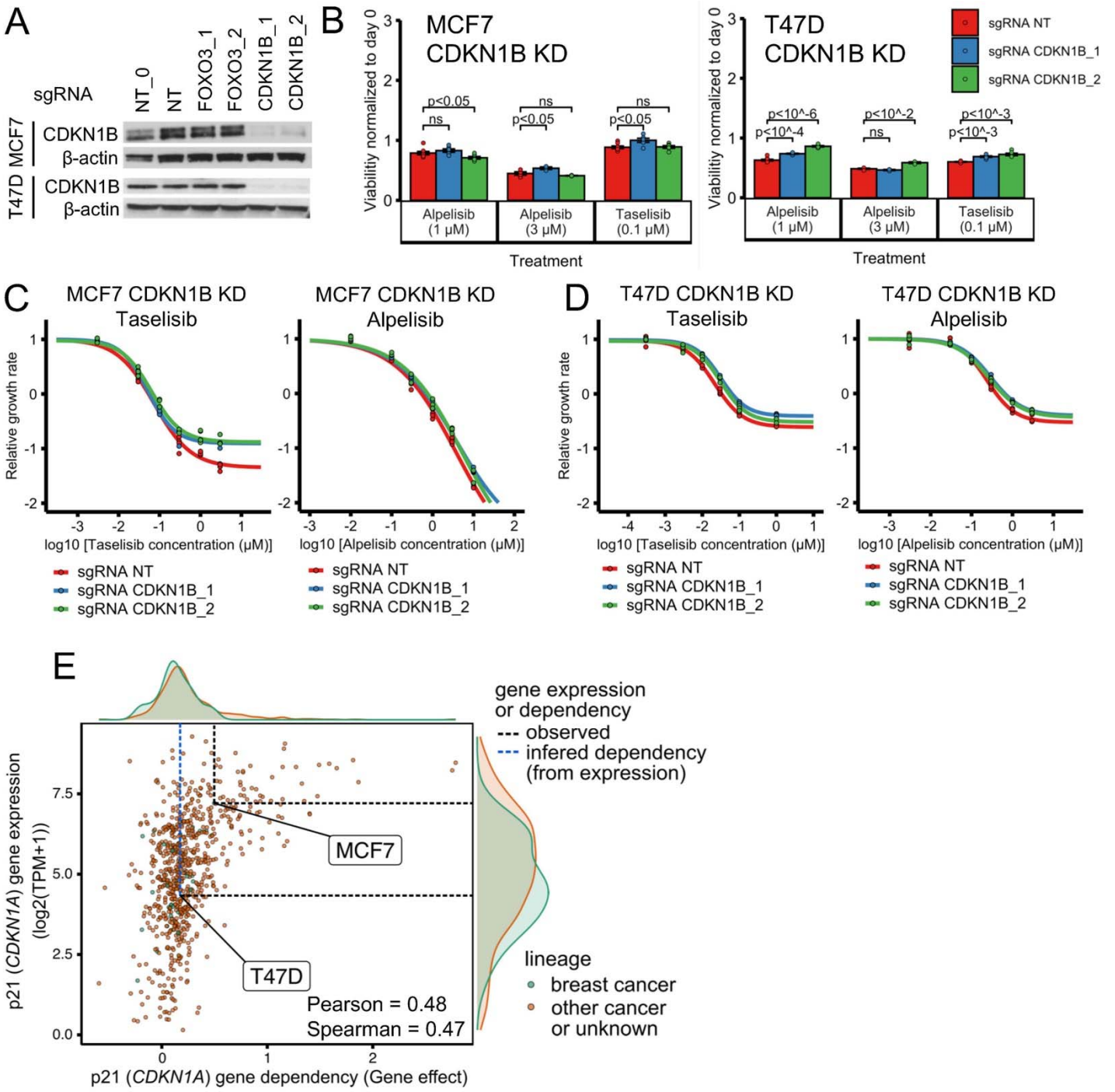

Fig. 4. CDKN1B (p27) knockdown does not have a strong effect on PI3Kα inhibitor sensitivity in ER+ breast cancer cell line models. (A) Stable cell lines were generated using CDKN1B CRISPR knockdown and showed reduced proteins levels of CDKN1B. NT and NT_0 are two distinct non-targeting control guides. CDKN1B_1 and CDKN1B_2 are two distinct guides targeting CDKN1B. NT, NT_0, FOXO3_1, and FOXO3_2 are the same guides as in Fig. 3. (B-D) CDKN1B knockdown does not strongly reduce sensitivity to PI3Kα inhibitors Alpelisib and Taselisib in ER+ breast cancer cell lines MCF7 and T47D. The same experimental procedures as in panels B-D of Fig. 3 were used for panels B-D of this figure. Cell viability was measured before and after 6 days of drug treatment using CellTiter-Glo. Group comparisons between groups were done using an unpaired, two-sided t-test (panel B). Panels C and D calculate the relative growth rate with respect to DMSO control. (E) Sensitivity to p21 (CDKN1A) knockout in CRISPR/Cas-9 loss-of-function screens (DepMap) is strongly correlated with p21 gene expression. We hypothesize that the activity of p21 is behind the lack of a strong effect of p27 knockout on PI3Kα inhibitor sensitivity. Based on T47D's p21 gene expression, the expected growth effect of p21 gene knockout on T47D is inferred to be smaller than that on MCF7. Sensitivity to gene knockout is measured using gene effect, which is such that gene effect=0 means no effect and gene effect=-1 is the median effect of

known common essential genes. Inferred gene effect is shown with a dashed blue line; gene expression or gene effect from the dataset is shown with a dashed black line.

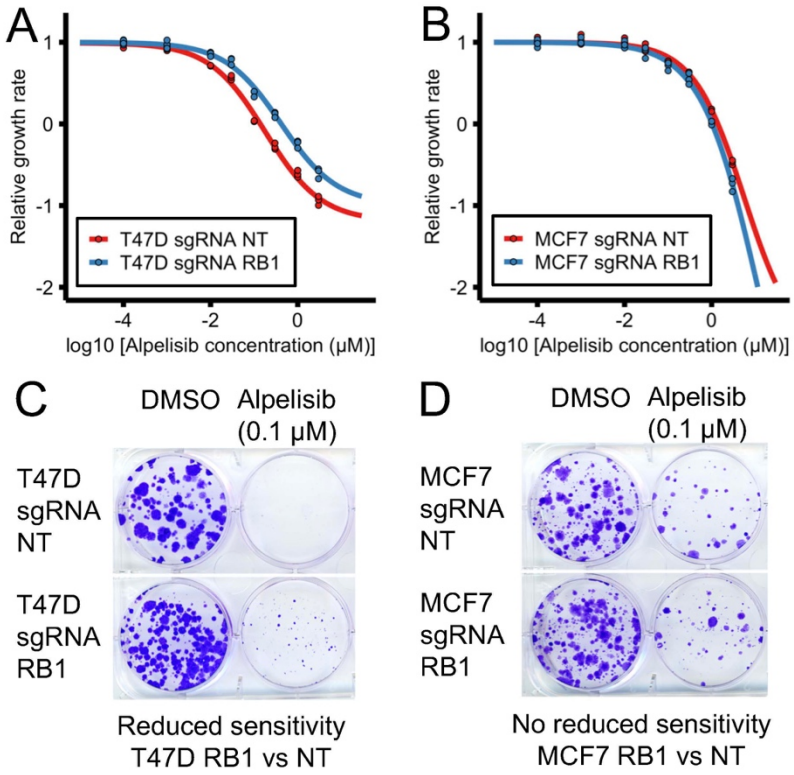

Fig. 5. RB1 knockdown can reduce sensitivity to PI3Kα inhibitors in ER+ breast cancer cell line models. RB1 knockdown in T47D (panels A and C) but not MCF7 cells (panels B and D) results in a reduced sensitivity to PI3Kα inhibitor Alpelisib in short-term and long-term assays. Cell viability was measured using a CellTiter-Glo assay before and after 6 days of drug treatment. Relative growth rate was calculated compared to the DMSO control treatment (panels A and B). Colony formation assay was performed after 30-40 days of drug treatment.

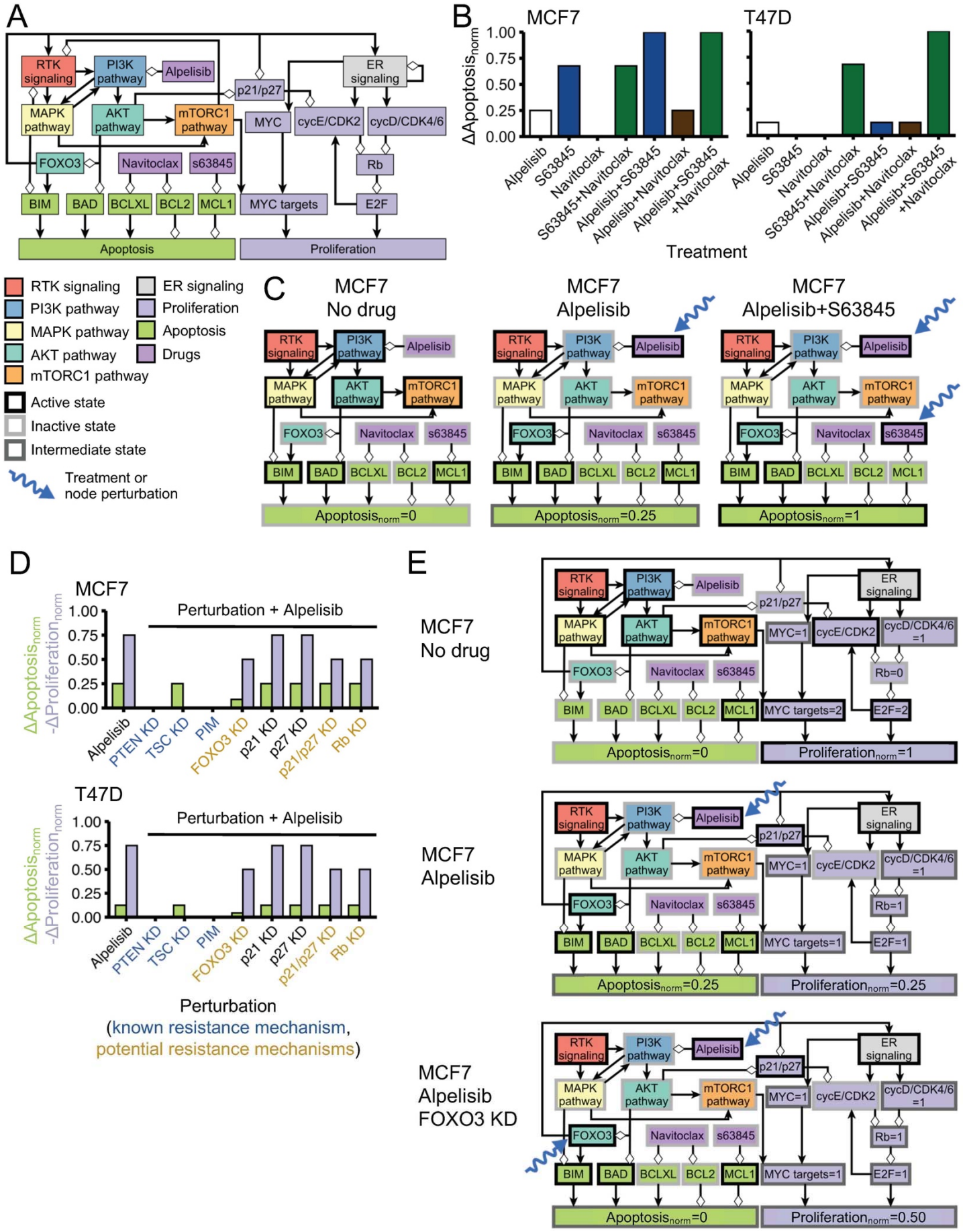

Fig. 6. Cell-line-specific network models reproduce the efficacy of combined PI3Kα inhibitors and BH3 mimetics

and the effect of PI3Kα inhibitor resistance mechanisms in MCF7 and T47D. (A) Condensed representation of the network model in which the cell-line specific models are based. The condensed representation includes nodes denoting pathways (RTK signaling, PI3K pathway, MAPK pathway, AKT pathway, mTORC1 pathway, and ER signaling), biological outcomes (apoptosis, proliferation), and drugs or proteins of interest for this work (e.g. Alpelisib, S63845, Navitoclax, FOXO3, p21/p27, and Rb). A more complete representation of the network model is shown in Supp. Fig. S4. (B-C) MCF7-specific and T47D-specific network models reproduce the difference in cell death responses to BH3 mimetics, Alpelisib, and their combination seen in these cell lines. The model results in panel B are comparable to the experimental results in Fig. 1E (MCF7) and 2C (T47D) (see Supp. Fig S6). We show the state of the nodes that influence $Apoptosis$ in response to Alpelisib, BH3 mimetics, and their combination for the case of MCF7 (panel C) and T47D (Supp. Fig S5B). (D-E) Cell-line specific network models reproduce the drug resistance effect of PI3Kα inhibitor resistance mechanisms. Simulations in which a PI3Kα inhibitor resistance mechanism is active show an increased survivability (reduced $Proliferation$ and/or increased $Apoptosis$) compared to the case of Alpelisib alone (panel D). We show the state of the nodes that influence $Apoptosis$ and $Proliferation$ in response to Alpelisib, FOXO3 knockdown, and their combination for the case of MCF7 (panel E) and T47D (Supp. Fig S5D). The models encode the biological outcomes of cell death and proliferation using $Apoptosis_{norm}$ and $Proliferation_{norm}$, respectively, which are a weighted and normalized (between 0 and 1) measure of the state of the nodes $Apoptosis$ and $Proliferation$. Starting from a cancerous state of each model, we perform 10,000 simulations in which the specified treatment or perturbation is maintained throughout the simulation, and obtain the average value of $Apoptosis_{norm}$ and $Proliferation_{norm}$ at the end of the simulations. $\Delta Apoptosis_{norm}$ and $\Delta Proliferation_{norm}$ of a perturbation denote the difference with respect to the case of no perturbation ($Apoptosis_{norm} = 0$, $Proliferation_{norm} = 1$), and are such that decreased survivability means an increase in $\Delta Apoptosis_{norm}$ or $-\Delta Proliferation_{norm}$.